Geomech. Geophys. Geo-energ. Geo-resour. (2023) 9:117
https://doi.org/10.1007/s40948-023-00658-5

RESEARCH

Depositional model of clastic and carbonate rocks in a continental rift basin: a case study of the Paleogene Shahejie Formation in the Cangdong Depression, Bohai Bay Basin

Shaoze Zhao · Yong Li · Yingjiao Xu · Tanfeng Zhang · Liangang Mu · Xuesong Wu · Xiugang Pu · Peng Yang · Xuehua Yuan

Received: 17 February 2023 / Accepted: 6 September 2023

Abstract The study of a clastic and carbonate rock depositional model in a continental rift basin is helpful to better understand the sedimentary processes active in continental rift basins. However, the spatiotemporal evolution characteristics and controlling factors of clastic and carbonate rocks in continental rift basins are still unclear. Therefore, the sedimentary characteristics of the clastic and carbonate rocks in the Paleogene Eocene Shahejie Formation (Es) are analysed via seismic, well log, core, thin section, and geochemistry data. Then, the impacts of tectonic movement, sediment supply and hydrologic conditions on sedimentary characteristics are discussed, and a depositional model is finally established. Five 3rd-order sequences, named SQ1–SQ5 from bottom to top, are identified in the Es. Fan delta, braided delta, meandering river delta, and lake sedimentary systems are identified in the Es; clastic rock sedimentary systems are identified in SQ1–SQ4, while concurrent clastic and carbonate rock sedimentary systems are identified in SQ5. During the SQ1–SQ4 period, the palaeogeomorphology formed by differential faulting activity or fault interactions and the inherited palaeogeomorphology resulted in different distributions of the sedimentary systems. The changes in accommodation space and sediment supply caused by tectonic movement led the delta to prograde or disappear. During the SQ5 period, the clastic rock sedimentary systems underwent a transition into clastic rock and carbonate rock sedimentary systems as a result of rift weakening, broad crustal thermal subsidence, sediment supply reduction and high-salinity lake water. This study provides a typical case for the evolution characteristics of the clastic rock and carbonate rock systems in continental rift basins, identifies changes in the tectonic, sediment supply, and hydrologic characteristics during their mutual transformations, and provides an important reference for hydrocarbon reservoir prediction.

Article highlights

(1) Fan delta, braided delta, meandering river delta, and lake sedimentary systems are identified in five 3rd-order sequences of the Shahejie Formation.

S. Zhao (✉) · Y. Li (✉) · T. Zhang
College of Earth Sciences, Chengdu University of Technology, Chengdu 610059, China
e-mail: zhaosz@cdut.edu.cn

Y. Li
e-mail: liy@cdut.edu.cn

S. Zhao
Geology Centre for Postdoctoral Studies, Chengdu University of Technology, Chengdu 610059, China

Y. Xu
College of Earth Sciences, Hebei GEO University, Shijiazhuang 050031, China

L. Mu · X. Wu · X. Pu · P. Yang · X. Yuan
PetroChina Dagang Oilfield Company, Tianjin 300280, China

Published online: 15 September 2023

(2) Clastic rock sedimentary systems appear in SQ1–SQ4, while clastic rock and carbonate rock sedimentary systems appear simultaneously in SQ5.
(3) The impacts of tectonic movement, sediment supply and hydrologic conditions jointly controlled the sedimentary process of the Shahejie Formation.
(4) A depositional model of clastic and carbonate rocks is established in the Cangdong Depression.

Keywords Continental rift basin · Cangdong Depression · Clastic rock sedimentary system · Syn-rift sedimentation · Sequence boundaries · Petrophysical analysis · Depositional model

1 Introduction

Continental rift basins are generated by the break-up of a continental landmass and are elongated depressions perpendicular to the direction of extensional tectonic forces, forming a series of linked half-grabens (Rosendahl 1987; Xie and Ren 2013; Goswami and Ghosh 2020). As a result of frequent tectonic movements, a continental rift basin is characterized by limited distribution, multiple provenances, uneven subsidence, multiple depocentres, diverse types of sedimentary systems, narrow facies belts and abrupt facies changes (Wang et al. 2011). A continuous syn-rift cycle includes an initial rifting phase, a fault interaction and linkage phase, an intense rifting phase, and a failed rifting phase (Gawthorpe and Leeder 2000; Morley 2002; Wang et al. 2015). Clastic rock sedimentary systems in continental rift basins at different stages have been studied a lot, and it is considered that the clastic rocks are mainly deposited in deltas or beach bars of lake environments in continental rift basins (Olsen 1990; Wang et al. 2015; Wu et al. 2015a, b; Ge et al. 2018; Li et al. 2019, 2022; Hou et al. 2019; Jia et al. 2019; Yang et al. 2021). Moreover, researchers considered that the palaeogeomorphologic features and tectonic evolution controlled the spatiotemporal distributions of the clastic rock sedimentary systems in continental rift basins (Olsen 1990; Wu et al. 2015a, b; Li et al. 2019; Hou et al. 2019). Carbonate rocks are common in continental rift basins, but studies on carbonate rock sedimentary systems in continental rift basins are less common than those on clastic rock sedimentary systems (Gierlowski-Kordesch 2010; Muniz and Bosence 2018; Liu et al. 2020a). In addition, the clastic rock and carbonate rock sedimentary systems of a continental rift basin have rarely been studied as a whole. Liu et al. (2020a) argued that palaeogeomorphologic features and hydrologic conditions controlled the development of carbonate sedimentary systems in continental rift basins. Liu et al. (2020b) believed that deltas occurred at the edge of the basin and carbonate banks developed at the intrabasinal uplift during the deposition of the first member of the Paleogene Eocene Shahejie Formation (Es) in the Zhanhua Depression, Bohai Bay Basin (BBB), which explained the spatial distributions of the clastic and carbonate rock sedimentary systems to a certain extent but did not clarify the temporal evolution characteristics between the two. What are the spatial–temporal evolution characteristics of these two systems? What are the factors controlling the evolution of these two systems? Exploring these issues is important for us to better understand the depositional process and model in continental rift basins.

The BBB is a rift basin that is controlled by the interaction between the Pacific plate and Eurasian continent and deep material activity (Chen et al. 1984; Watson et al. 1987; Northrup et al. 1995; Allen et al. 1997; Ren et al. 2002). The Cangdong Depression (CDD) is a part of the BBB and is composed of several connected half-grabens. Clastic rocks and carbonate rocks were deposited contemporaneously in the Paleogene Es; therefore, the CDD is an ideal area for studying the sedimentary characteristics of clastic and carbonate rocks and their controlling factors. The CDD is also an important hydrocarbon-rich depression. Great advances have recently been accomplished in conventional and unconventional hydrocarbon exploration in the CDD (Zhao et al. 2018, 2019). Many structural and lithologic oil reservoirs have been discovered in the CDD, and the reservoirs are sandstones of the Paleogene Kongdian Formation (Zhao et al. 2018). Moreover, the shale oil of the Kongdian Formation has realized industrial development (Zhao et al. 2019). These advances have mainly focused on the Kongdian Formation, and Es has rarely been studied. Many hydrocarbon shows were discovered in the Es clastic rock and carbonate rock (Liu et al. 2010), showing potential

for hydrocarbon exploration. Therefore, clarifying the geological characteristics, especially the depositional model of the Es, is necessary. In summary, the study of the depositional model of the Es in the CDD has great theoretical importance for the study of clastic and carbonate rock depositional models in a continental rift basin and in hydrocarbon exploration in the CDD.

This paper aims to (1) clarify the types, provenances and distributions of the sedimentary systems in the 3rd-order sequence of the Es; (2) discuss the factors controlling the sedimentary characteristics of the Es; and (3) establish a depositional model of the Es.

2 Geological setting

The NNE-trending CDD is in the southern Huanghua Subbasin in the BBB, and it is bounded by the Kongdian bulge structural belt, Dongguang bulge structural belt, Cangxian uplift and Xuhei bulge. It gradually expands such as a horn (Fig. 1a, b). The Cangdong fault the western boundary fault, with a dip to the ESE and strike to the NNE (Fig. 1c). The Xuxi fault is the eastern boundary fault, which dips WNW and strikes NNE (Fig. 1c). The NNE-trending Kongdian bulge structural belt is the most prominent bulge zone in the CDD, with the Changzhuang subdepression to the east, the Cangdong subdepression to the west and the Nanpi

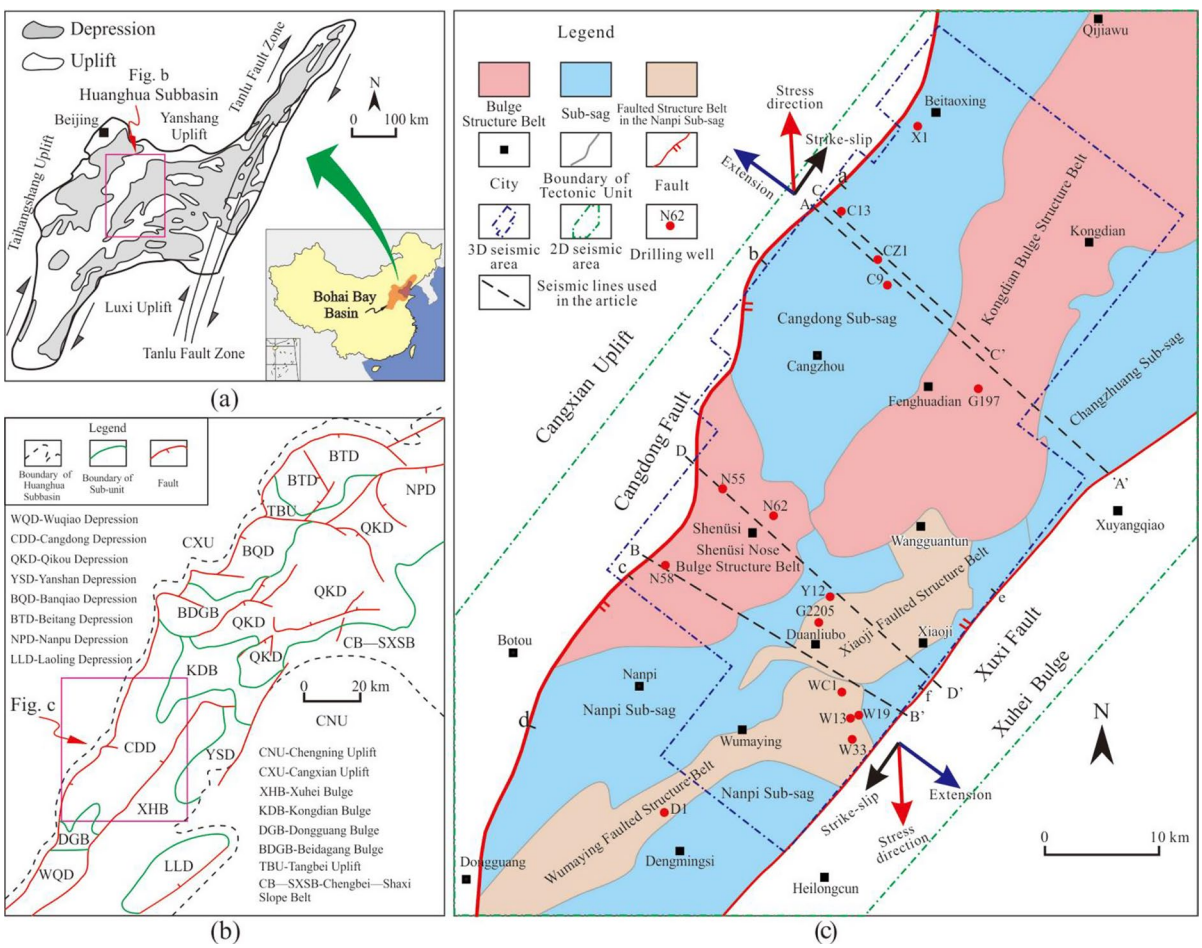

Fig. 1 Geological background of the CDD. **a** Location of the BBB and Huanghua subbasin. **b** Subunits of the Huanghua subbasin and location of the CDD. **c** Divisions of the structural units of the CDD. Points a–f on the boundary fault are locations of the measurement points of the fault activity rates

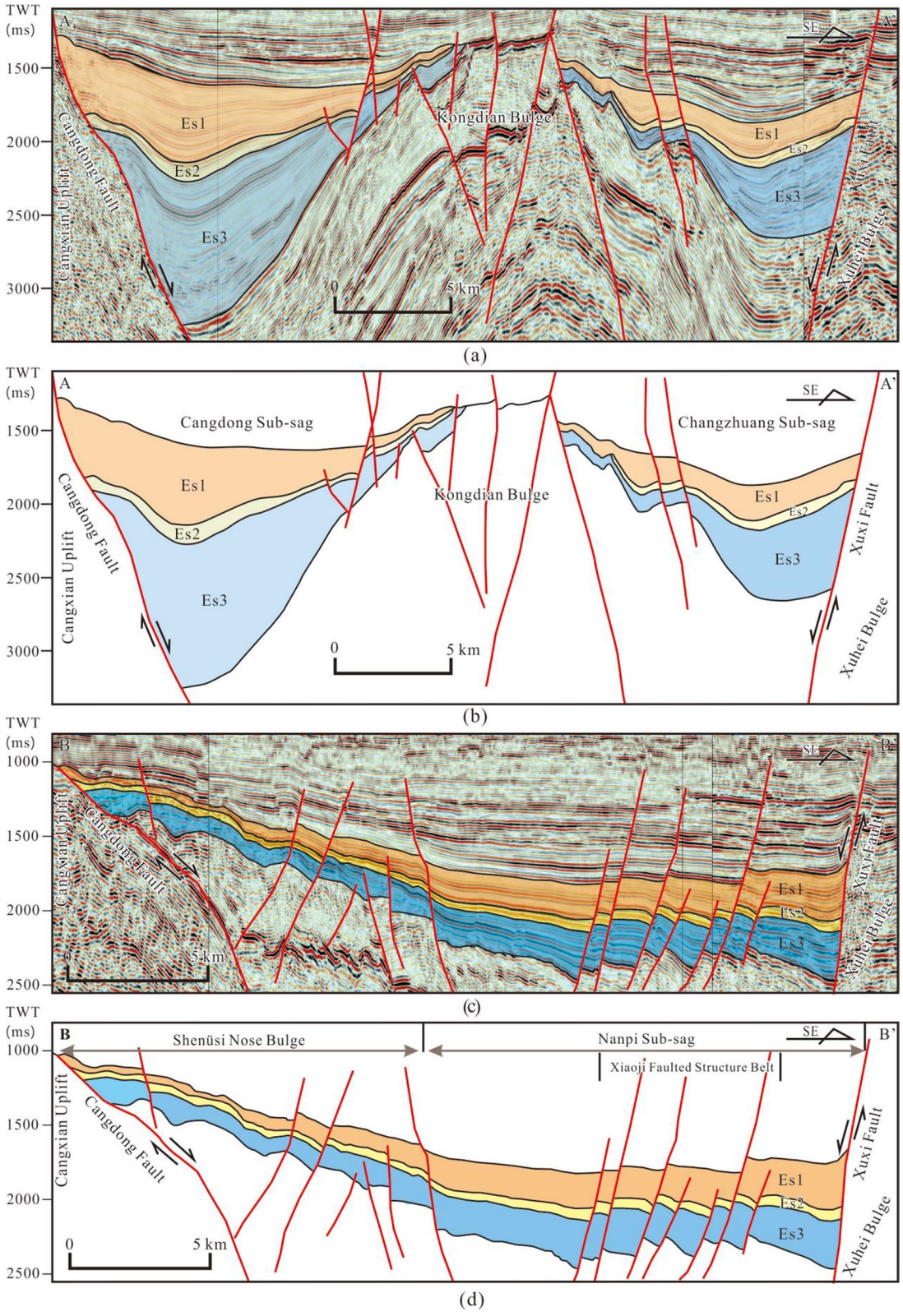
TWT
(ms)
1500
2000
2500
3000
A
A'
SE
Es1
Es2
Es3
Kongdian Bulge
Cangdong Fault
Cangxian Uplift
Xuxi Fault
Xuhei Bulge
0
5 km
(a)
Cangdong Sub-sag
Changzhuang Sub-sag
(b)
1000
B
B'
(c)
Shenüsi Nose Bulge
Nanpi Sub-sag
Xiaoji Faulted Structure Belt
(d)

◂**Fig. 2** **a**, **b** Tectonic framework characteristics of the northern CDD. **c**, **d** Tectonic framework characteristics of the southern CDD. See Fig. 1c for the locations of the seismic lines

subdepression to the south. These subdepressions are the main subsidence centres in the CDD (Fig. 1c). Two complex fault structures are present in the Nanpi subdepression, namely, the Wumaying and Xiaoji fault structure belts. In addition, the Shenüsi nose bulge structure belt is on the northwest of the Nanpi subdepression (Ye et al. 2013) (Fig. 1c). The CDD was affected by both extensional rifting and strike-slip faulting during the deposition of the Es (Ye et al. 2013) (Fig. 1c). Affected by the differential faulting activity along the two boundary faults, the CDD is divided into two different regions, namely, the northern-central region and the southern region. The northern-central region is "two half-grabens separated by one bulge" (Fig. 2a, b). The downthrown walls of the two boundary faults slip in opposite directions, forming a "rolling anticline" between the two faults, that is, the Kongdian bulge. The rolling anticline is formed under the mechanism of transverse bending folds in response to gravity (Ye et al. 2013). From the Shenüsi faulted nose to the southern CDD southwards, the faulting activity of the Xuxi fault is more intense than that of the Cangdong fault. The structure of this area is an asymmetric graben (Fig. 2c, d).

Es is subdivided into the third member (Es3), the second member (Es2) and the first member (Es1). The depositional period of Es3–Es2 was an interval of rifting. The depositional period of Es1 was a typical late rifting period since the activities of the boundary faults significantly weakened and broad crustal thermal subsidence occurred (Sopeña and Sánchez-Moya 1997; Zhang 2018; Hou et al. 2019). The maximum thicknesses of Es3, Es2, and Es1 are no more than 1500 m, 200 m, and 400 m, respectively (Fig. 3). Es3 consists of conglomerate, sandstone, and mudstone. Es2 consists of interbedded light grey conglomerate and sandstone, with minor mudstone. Es1 is stratified and overlies the top of Es2. In the lower part of Es1, clastic rocks dominate, followed by carbonate rocks. The clastic rocks consist of conglomerate and sandstone, with mainly medium- to fine-grained sandstone. The carbonate rocks are composed of bioclastic limestone. In the upper part of Es1, dark shale with a stable and continuous distribution dominates.

3 Data and methods

3.1 Data

Various data were collected from the Dagang Oilfield, PetroChina. (1) 3D seismic data and 2D seismic data. The inline and cross-line space of 3D seismic data is 25 m. The line space of 2D seismic data is about 1 km. These data cover the majority of the CDD (Fig. 1c), and 3D seismic data provided an interpretation scheme for the Es3 and Es1 bottom boundary. (2) Well log data. These data consist of geological well log data and geophysical well log data. The geological well log data included the lithological data and stratigraphic division data of approximately 100 wells. The geophysical well log data included the gamma ray curve, resistivity curve, and spontaneous potential curve. The article shows well logs from 12 wells (N55, C13, X1, CZ1, N58, Y12, G2205, W13, WC1, D1, N62, and G197) (Fig. 1c). (3) Data from core analysis. Heavy mineral data from 15 wells are used (The samples were crushed to 200 mesh and washed by shaking to obtain heavy minerals. The minerals were identified by microscopy, and the percentage of different heavy minerals was obtained by particle statistics). Rock fragment data from 5 wells were obtained by microscopic observation and statistics.

3.2 Samples and analytical methods

In addition to the data collected from the Dagang oilfield, cores of 24 wells were observed in the Dagang Oilfield, and the article shows core photographs from 9 wells (C13, X1, N58, Y12, G2205, W13, WC1, N62, G197) (Fig. 1c). Thin sections from 11 wells were observed by polarized light microscopy (Leica DM4500P) in the State Key Laboratory of Oil and Gas Reservoir Geology and Development Engineering, and the article shows microphotographs from 4 wells (G2205, WC1, W13, CZ1) (Fig. 1c). Geochemical analysis includes analysis of minor element concentrations and total organic carbon (TOC) contents. The minor element concentrations of 21 samples from 4 wells (C9, W33, W19, G197) were measured using a PerkinElmer ELAN DRC-e type inductively coupled plasma mass spectrometer (ICP−MS), and the

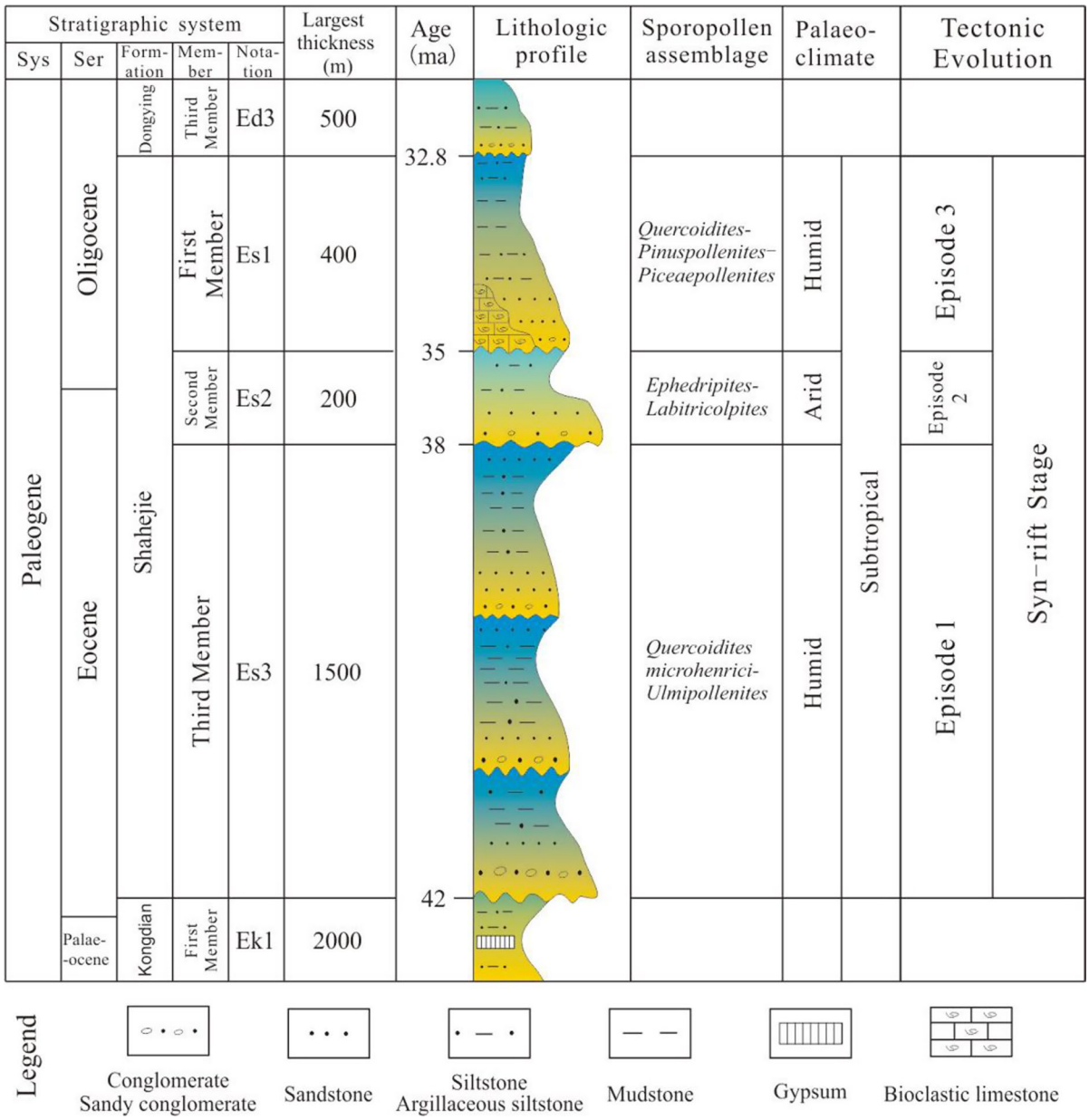

Fig. 3 Comprehensive stratigraphic column of the Es in the CDD showing the lithostratigraphy, sporopollen, palaeoclimate, and tectonic evolution. Sporopollen data are from Tong and Gu (1985)

TOC contents of 3 samples from 1 well (CZ1) were measured using a LECO CS-344 carbon–sulfur. Before the analysis, the samples were artificially crushed to smaller than 80 mesh in an agate mortar. These tests were completed at the Sichuan Coalfield Geology Bureau.

3.3 Research methods

The method of this study is to use seismic, well log, core, thin section and geochemistry data to establish the sequence stratigraphic framework of the Es and analyse the sedimentary system type, provenance and distribution of the sedimentary system. Finally,

the influence of tectonic movement, sediment supply and hydrological conditions on the sedimentary characteristics are discussed, and the depositional model is established. The novelty of this study is that a depositional model of the clastic and carbonate rocks of the Es in the CDD is established through multidata and multimethod analysis, which provides a typical case for the study of clastic and carbonate rocks sedimentary evolution in continental rift basins.

3.3.1 Research methods of sequence stratigraphy

The theoretical basis of sequence stratigraphy research is Continental sequence stratigraphy and classical sequence stratigraphy (Hanneman and Wideman 2010), the key of which is to identify the sequence boundary (unconformity and its corresponding conformity), then divide the 3rd-order sequence and establish the sequence framework. Two types of data are used to identify sequence boundaries: (1) Seismic profile data: the sequence boundary in the seismic profile shows the reflection characteristics of onlaps, downlaps, toplaps and truncations. (2) Well log data: the lithology and its combination characteristics revealed by well log data would change significantly above and below the sequence boundary.

3.3.2 Research methods of sedimentary system type

The analysis of sedimentary system type is based on the facies analysis (Miall 1984) and the descriptive sedimentary terminology of Collinson et al. (2006) and Zhu (2008). Sedimentary system types are identified by cores, thin sections, geophysical well logs and seismic reflection profiles. Among them, the lithology, sorting, roundness and sedimentary structure (plane structure and bedding structure) are observed by using cores and thin sections to comprehensively judge the sedimentary facies type. In the areas without cored wells, the sedimentary facies types were identified based on the shapes of geophysical well logs (bell-shaped, box-shaped, funnel-shaped, finger-shaped). In addition, the external morphology and internal reflection characteristics of the seismic profiles are used to determine specific types of sedimentary facies.

3.3.3 Research methods of provenance

Sediments from different provenances have different assemblage characteristics of heavy minerals (magnetite, tourmaline, zircon, etc.) and rock debris (magmatic rocks, metamorphic rocks, and sedimentary rocks) (Li et al. 2019). Seismic foreset reflection can reflect the direction of the palaeocurrent. Therefore, the macroscopic provenance direction of the CDD is analysed by heavy mineral assemblages, rock debris assemblages and seismic profiles. On this basis, the detailed distribution of provenance and sand bodies are determined according to the spatial variation in the percentage of sandstone in sedimentary strata.

3.3.4 Research methods for the distribution of sedimentary system

The theoretical basis of the distribution of sedimentary system is Walther's Law (Middleton 1973). Based on the sequence framework, combined with the analysis results of sedimentary system types and provenance, the distribution of sedimentary system of different sequences are determined.

3.3.5 Research methods for controlling factors of sedimentary characteristics

The sedimentary characteristics of continental rift basins are influenced by tectonic movement, sediment supply, and hydrological conditions (Blair 1987; Leeder and Gawthorpe 1987; Olsen 1990; Wang et al. 2015; Wu et al. 2015a, b; Bayet-Goll et al. 2018; Li et al. 2019, 2022; Hou et al. 2019; Jia et al. 2019; Yang et al. 2021). Therefore, the controlling effects of these three factors on sedimentary characteristics are mainly discussed: (1) The burial time−depth of the bottom boundary of the Es3 and Es1 are extracted by using the 3D seismic data. A large (small) burial depth indicates a low (high) palaeotopography to judge the bottom palaeotopography of Es3 and Es1. Then, the spatiotemporal variation characteristics of tectonic activity intensity are judged combined with the fault activity rate, and the control effect of tectonic movement on the sedimentary system is discussed. (2) The spatiotemporal variations in sediment supply are analysed through the distribution of sand bodies, and then the control effect of sediment supply on the distribution of the sedimentary system is

discussed. (3) The salinity of ancient water bodies is restored by using minor element data, and then the control effect of hydrological conditions on the sedimentary system is analysed. Finally, the depositional model is established.

4 Results

4.1 Sequence stratigraphic framework

Sequence stratigraphic divisions can provide an isochronous framework for the research associated with sedimentary system (Catuneanu et al. 2009, 2011). Five 3rd-order sequences were recognized: Es3 corresponds to SQ1, SQ2, and SQ3 from bottom to top; Es2 corresponds to SQ4; and Es1 corresponds to SQ5; these sequences are separated by sequence boundaries SB1-SB6. There are onlaps and truncations below and above sequence boundaries in seismic reflection profiles (Fig. 4a, b). The sequence boundaries in wells are identified based on lithology and lithological association. Taking well N55 at the basin margin as an example, the first member of the Kongdian Formation (Ek1), which is dominated by thick red mudstone, is below SB1. Glutenite interbedded with thin mudstone is above SB1, indicating an abrupt change in the sedimentary environment. The strata underlying SB2, SB3, SB4 and SB6 are deposits with red, brown, and other oxidized colours, which indicate subaerial environments, while the overlying strata are dark sediments, which indicate underwater environments. The strata underlying SB5 are dominated by conglomerate deposits, while the overlying

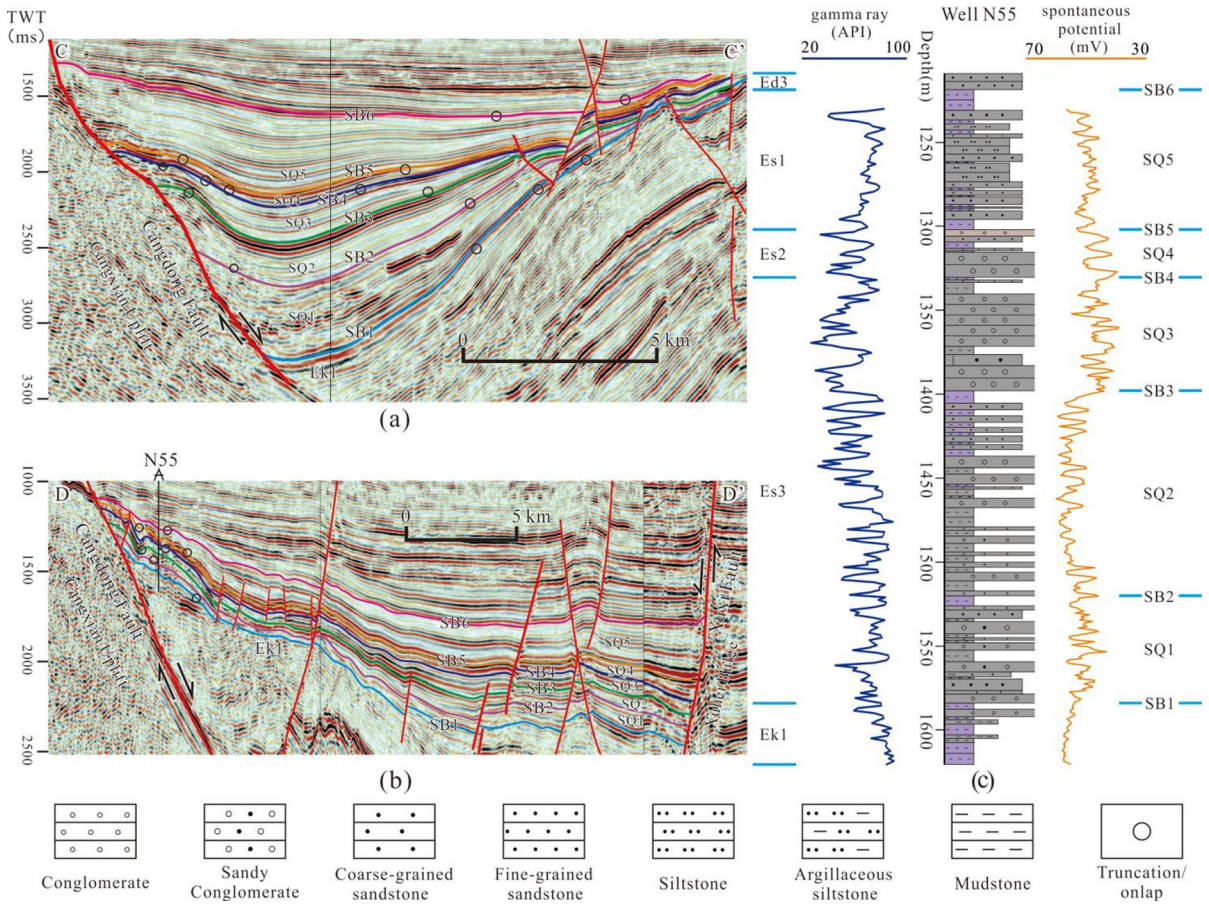

Fig. 4 Sequence stratigraphic division of the Es. **a**, **b** Sequence stratigraphic division on seismic profiles. **c** Sequence stratigraphic division on drilling well data. The locations of the seismic lines and drilling well is shown in Fig. 1c

strata are thin fine sandstone and siltstone interbedded with mudstone (Fig. 4c).

4.2 Sedimentary system

4.2.1 Fan delta

This sedimentary system is gravel-rich and fan-shaped due to alluvial fans directly entering stable water bodies from adjacent highlands. It is divided into subaerial and underwater parts. The subaerial part is composed of delta plain subfacies, while the underwater part is composed of delta front and prodelta subfacies (Holmes 1965; McPherson et al. 1987, 1988). Since prodelta deposits are similar to lacustrine deposits, which are generally made up of dark mudstone interbedded with thin siltstone, in this paper, they are classified as lacustrine deposits. Importantly, mudstone is generally deposited in marine or lake sedimentary environments. Palaeontological evidence shows that the BBB was a terrestrial lake during the deposition of the Es (Tong and Gu 1985). Therefore, the Es mudstone belongs to lacustrine deposits.

Fan delta plain subfacies are composed of distributary channels and interchannels. Distributary channel deposits are composed of variegated conglomerate with subtle normal grading. The conglomerate is poorly sorted and rounded, with granular support (Fig. 5a, c). Well logs from these deposits show dentate high-amplitude bell-shaped or box-shaped motifs (Fig. 5f). Interchannel deposits are dominated by thin purple−red (silty) mudstone (Fig. 5f). The fan delta front subfacies includes four types of microfacies: underwater distributary channels, interdistributary bays, mouth bars, and sheet sand, with underwater distributary channels dominating. The mouth bar is poorly developed since the channels of the fan delta front frequently change their routes. Underwater distributary channel deposits are generally composed of grey sandy conglomerate, conglomeratic sandstone, medium- to coarse-grained sandstone, and fine-grained sandstone, with grain sizes gradually fining upwards (Fig. 5b). The gravel in sandy conglomerate and conglomeratic sandstone has good roundness, and massive bedding is identified (Fig. 5d). Sandstone generally has parallel bedding and massive bedding (Fig. 5e). Their well logs are also jagged bell-shaped or box-shaped geometries, similar to those of fan delta plain distributary channel deposits, although the amplitudes are smaller (Fig. 5g). Interdistributary bay deposits are composed of dark mudstone deposits. Sheet sand deposits with thin individual layers are composed of grey−black siltstone, and well logs from sheet sandstone deposits mostly represent finger-like or spike-like shapes (Fig. 5h). Fan deltas feature wedge-shaped, internally disordered foreset reflections on seismic profiles. The wedge-shaped disordered reflection structure at the root corresponds to the plain of the fan delta, while the foreset structure in the middle and front ends corresponds to the fan delta front (Fig. 5i).

4.2.2 Braided delta

This sedimentary system developed due to the progradation of the braided river into a stagnant lake, which is a unique type of delta that is intermediate between the coarse-grained fan delta and the fine-grained meandering river delta (McPherson et al. 1987). Braided deltas are also divided into braided delta plain (subaerial part) and braided delta front (underwater part).

The braided delta plain subfacies consist of two types of microfacies: distributary channels and interchannels. Distributary channel deposits consist of variegated conglomerate, conglomeratic sandstone, and sandston, forming a normal cycle structure (Fig. 6a, e, f). The gravel of conglomerate in braided delta plain deposits has a smaller diameter and better roundness and sorting than that in fan delta plain deposits (Figs. 5c, 6f), and massive bedding and parallel bedding are present in conglomerate and sandstone (Fig. 6e, f). Well logs of these deposits often show medium- to low-amplitude box-shaped and bell-shaped or dentate box-shaped and bell-shaped deposits (Fig. 6l). Interchannel deposits that are formed by the migration of the distributary channel are dominated by brown−red mudstone (Fig. 6d) and argillaceous siltstone, thus forming a fining-upwards normal cycle with the glutenite of the distributary channel (Fig. 6a). The braided delta front is composed of an underwater distributary channel, interdistributary bay, mouth bar and sheet sand. Underwater distributary channel deposits consist of massive bedding in medium-grained and fine-grained sandstone, forming a fining-upwards normal cycle with a scouring

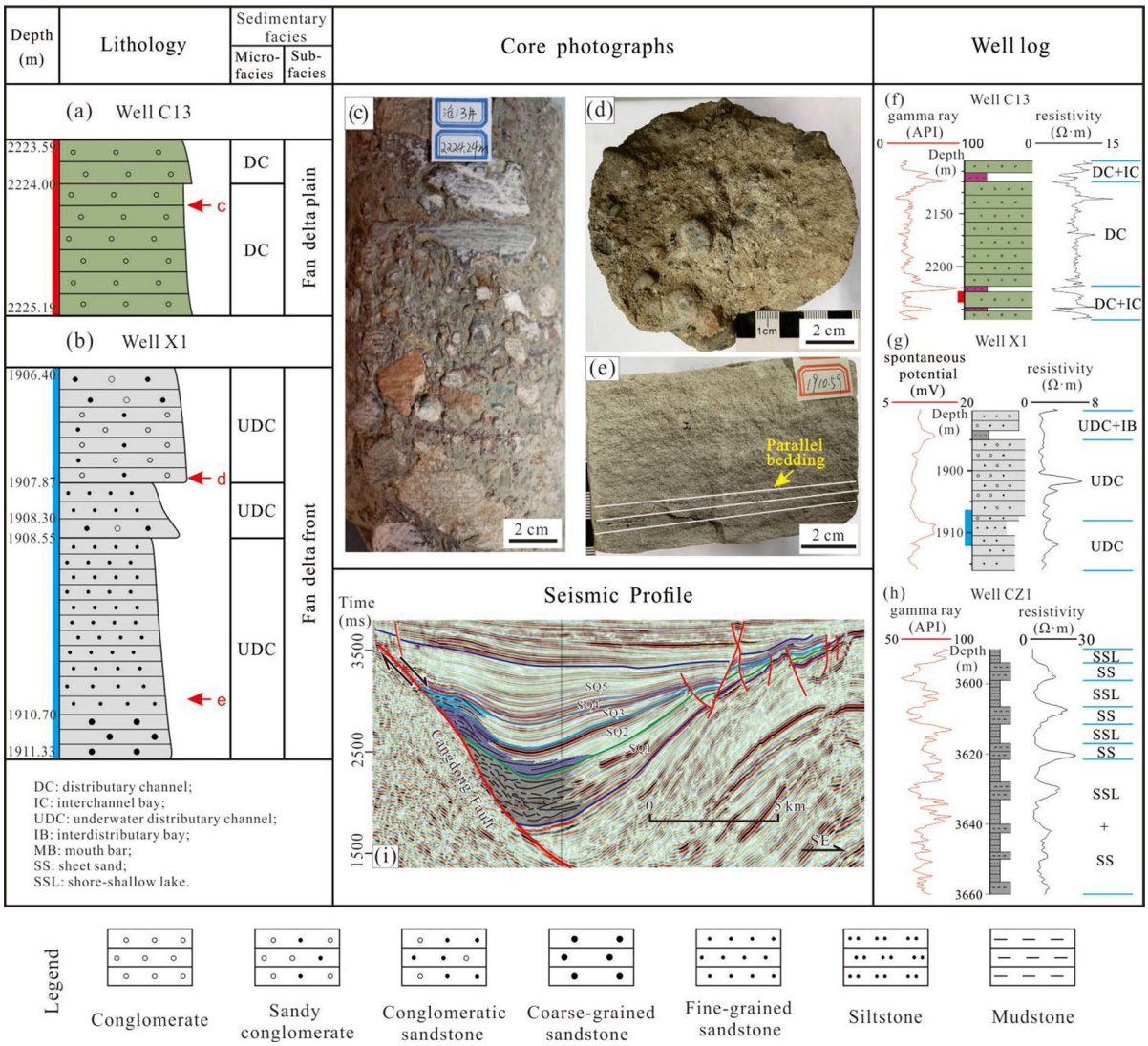

Fig. 5 Cores, well logs, and seismic reflection characteristics of the fan delta. **a**, **b** Stratigraphic columns of fan delta cores from the Es. **c** Variegated conglomerate and gravel, poorly sorted and rounded. **d** Grey conglomeratic sandstone with massive bedding and well-rounded gravel. **e** Grey fine-grained sandstone with parallel bedding. **f–h** Well log characteristics of the fan delta deposits. **i** Fan delta seismic reflection characteristics. The locations of drilling wells are shown in Fig. 1c

surface at the bottom (Fig. 6b, g). Well logs from these deposits generally represent medium- to low-amplitude box-shaped and bell-shaped geometries (Fig. 6m) and resemble those from distributary channel deposits. Interchannel deposits are generally composed of light grey or grey−green argillaceous siltstone, mudstone, and siltstone, with massive bedding (Fig. 6b, g). Deposits of the mouth bar are generally composed of sandstone with reverse rhythm (Fig. 6c). Carbonaceous laminations (Fig. 6h), parallel bedding, tabular cross-bedding (Fig. 6i) and small trough cross-bedding (Fig. 6j) are shown in these deposits. Well logs from mouth bar deposits mainly represent moderate-amplitude funnel-shaped geometries (Fig. 6n). Sheet sand deposits generally consist of fine-grained sandstone and siltstone, which are generally well sorted and rounded after repeated elutriation by lake currents or waves (Fig. 6k). Due to the high concentration of calcium ions in lake water, sandstone

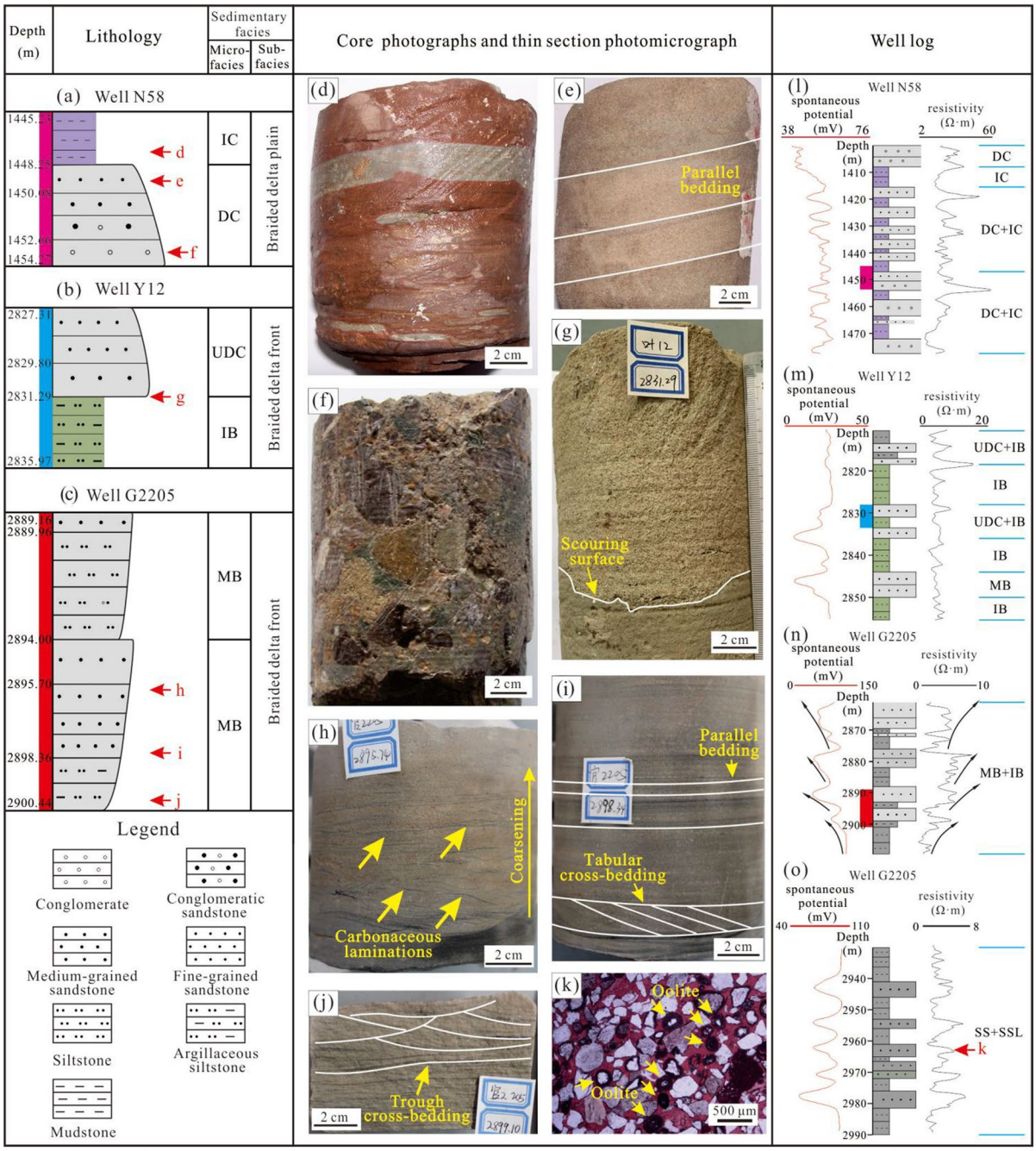

Fig. 6 Cores, thin section, well logs of braided delta. **a–c** Stratigraphic columns of braided delta cores from the Es. **d** Brown−red and grey−green mudstone. **e** Grey fine-grained sandstone with parallel bedding. **f** Variegated conglomerate with massive bedding and better sorting and roundness than that in Fig. 5c. **g** Lower part: grey−green argillaceous siltstone; upper part: grey medium-grained sandstone with a scouring surface. **h** Light grey fine-grained sandstone with carbonaceous laminations, coarsening-upwards grain size. **i** Light grey fine-grained sandstone, with tabular cross-bedding at the bottom, parallel bedding in the upper part. **j** Light grey argillaceous siltstone with small trough cross-bedding. **k** Oolitic fine-grained sandstone, with arenes in oolite cores. **l–o** Well log characteristics of the braided delta deposits. The locations of drilling wells are shown in Fig. 1c

often contains oolites with sand cuttings in cores (Fig. 6k). Thin sheet sand is often intercalated with lacustrine dark mudstone and appears as finger-like or spike-like shapes in well logs (Fig. 6o).

4.2.3 Meandering river delta

This sedimentary system refers to the delta system that is formed by meandering rivers flowing into lakes for a long distance. Compared with the near-source sand- and gravel-rich braided delta and fan delta, the meandering river delta sediments have finer grain sizes. Well-sorted and rounded medium-fine sandstone, siltstone and mudstone dominate and have high structural and compositional maturity.

The meandering river delta consists of only the delta front subfacies, which is subdivided into underwater distributary channels, interdistributary bays, mouth bars and sheet sand. Since the meandering river delta front is connected with the braided delta front, the sheet sand microfacies of the meandering river delta front has characteristics similar to those of the braided delta front. Therefore, they are not described in this section. Deposits of underwater distributary channels and interdistributary bays constitute a fining-upwards sedimentary rhythm (Fig. 7a). Underwater distributary channel deposits primarily consist of fine-grained sandstone (Fig. 7d, e), which is generally well sorted and rounded and has high structural and compositional maturity (Fig. 7e). Similar to those of underwater distributary channels in other types of deltas, well logs from these deposits mainly show medium- to low-amplitude box-shaped or dentate box-shaped geometries (Fig. 7i, j). Interdistributary bay deposits are dominated by green−grey mudstone or silty mudstone (Fig. 7c). Mouth bar deposits are dominated by silty mudstone (Fig. 7h), fine-grained sandstone (Fig. 7g), and medium-grained sandstone (Fig. 7f), showing reverse-grained sedimentary rhythm on the sedimentary profile (Fig. 7b). The sandstone is sub-rounded and well sorted and contains oolites with sand cuttings in the cores due to repeated elutriation by lakes and rivers (Fig. 7f, g). These deposits are funnel-shaped in well logs (Fig. 7j, k). The gentle geomorphology and low-angle foreset reflection can be seen on the seismic profile (Fig. 7l), which is typical of a meandering river delta front.

4.2.4 Lake

Sandy beach bars, carbonate banks, shore-shallow lakes, and semi-deep to deep lake subfacies can be recognized in this sedimentary system.

Affected by lake waves, the banded or sheet-like clastic sands or carbonate rocks of the beach bar subfacies are often continuously distributed (Song et al. 2018). Sandy beach bars can be divided into the main body of the bar microfacies and the bar margin microfacies because of the different hydrodynamic conditions. Deposits from the main bodies of bars are composed of different-grained sandstones with high compositional and structural maturity, showing a coarsening-upwards reverse-grained sedimentary rhythm (Fig. 8a). These sediments exhibit parallel bedding, cross-bedding, and wavy cross-bedding (Fig. 8b–d). In areas where the sandy beach bar and carbonate bank are adjacent, gastropod fossils are widespread in the sandstone (Fig. 8c). Argillaceous sediments dominate the bar margin (Fig. 8h). In well logs, the bar margin and bar main body are represented by dentate medium- to low-amplitude funnel-shaped structures (Fig. 8h). Carbonate bank deposits are composed of grey−yellow–brown bioclastic limestone, in which dissolved pores are common (Fig. 8e). These deposits always have high resistivity values and low spontaneous potential values (Fig. 8i).

Shore-shallow lake deposits are dominated by light colour mudstone or silty mudstone with horizontal bedding and massive bedding. Shore-shallow lacustrine mudstone is a poor source rock or not a source rock due to its low TOC content. Deposits of Semi-deep to deep lake are mainly distributed in SQ1–SQ3 and SQ5. They are dominated by thick dolomitic mudstone (Fig. 8f, g), calcareous mudstone, and dark mudstone (Fig. 8j). The sediments with high GR values and high TOC contents are important source rocks (Fig. 8j).

4.3 Provenance

Provenance identification is vital in palaeogeographic reconstructions (Haughton et al. 1991). The provenances of SQ1, SQ2 and SQ3 are consistent; they show only progradation or retrogradation of sand bodies. Therefore, in this paper, only the provenance of SQ3 is analysed in detail to represent the provenance system of Es3.

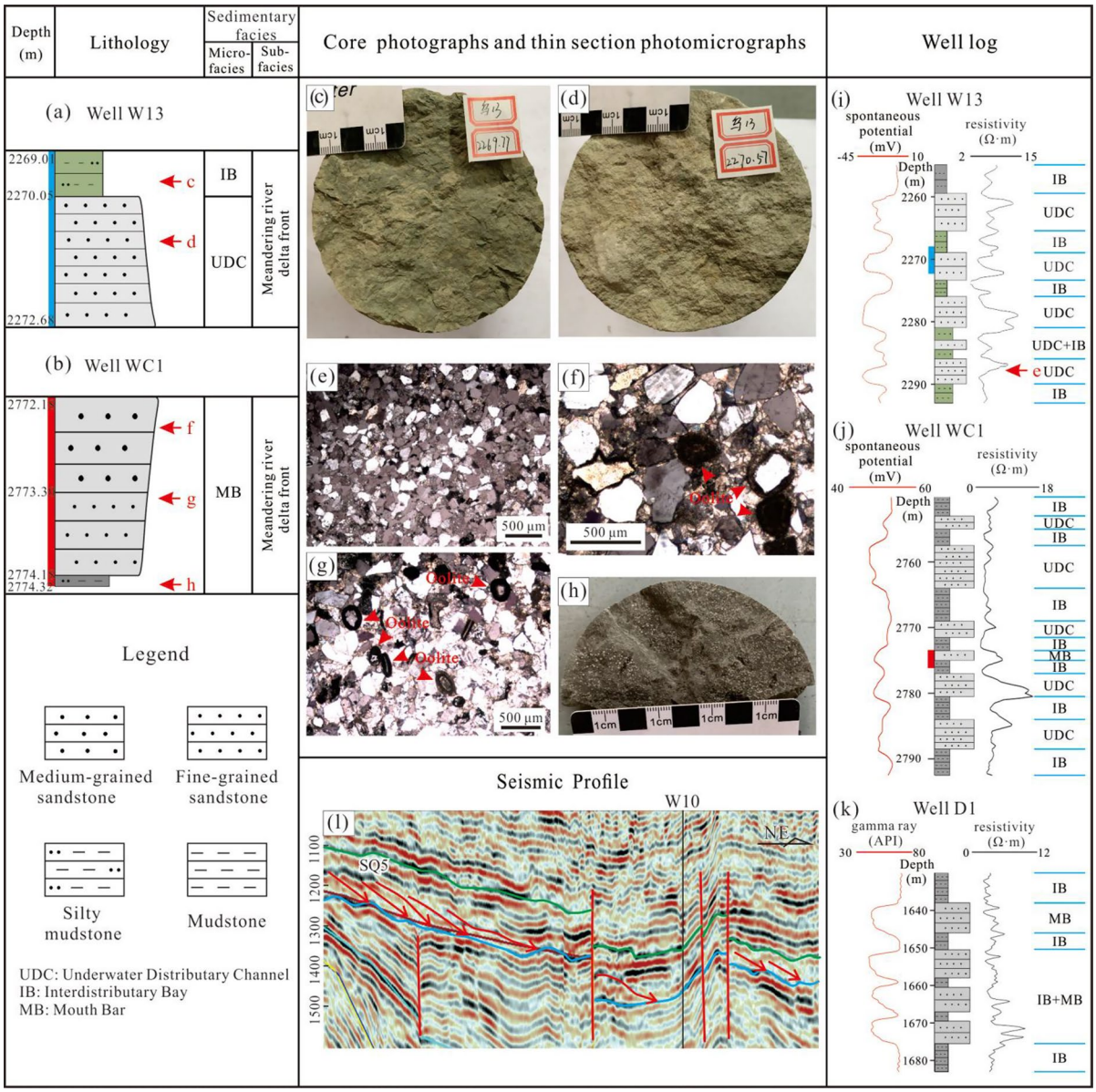

Fig. 7 Cores, thin sections, well logs and seismic reflection characteristics of the meandering river delta. **a**, **b** Stratigraphic columns of meandering river delta cores from the Es. **c** Grey−green silty mudstone. **d** Grey−white fine-grained sandstone with massive bedding. **e** Fine-grained feldspar sandstone, well sorted and rounded. **f** Oolitic medium-grained sandstone, well sorted and rounded, arene is in the core of oolite. **g** Oolitic fine-grained sandstone. **h** Grey−black argillaceous siltstone. **i**–**k** Well log characteristics of the meandering river delta deposits. **l** Seismic profile with foreset reflection. The locations of drilling wells are shown in Fig. 1c

There were four major provenances in the CDD during the depositional period of SQ3, namely, the Cangxian provenance, Xuhei provenance, Kongdian provenance, and Dongguang provenance. Garnet, magnetite and zircon dominate in the Cangxian provenance, with minor hornblende. Garnet, zircon and

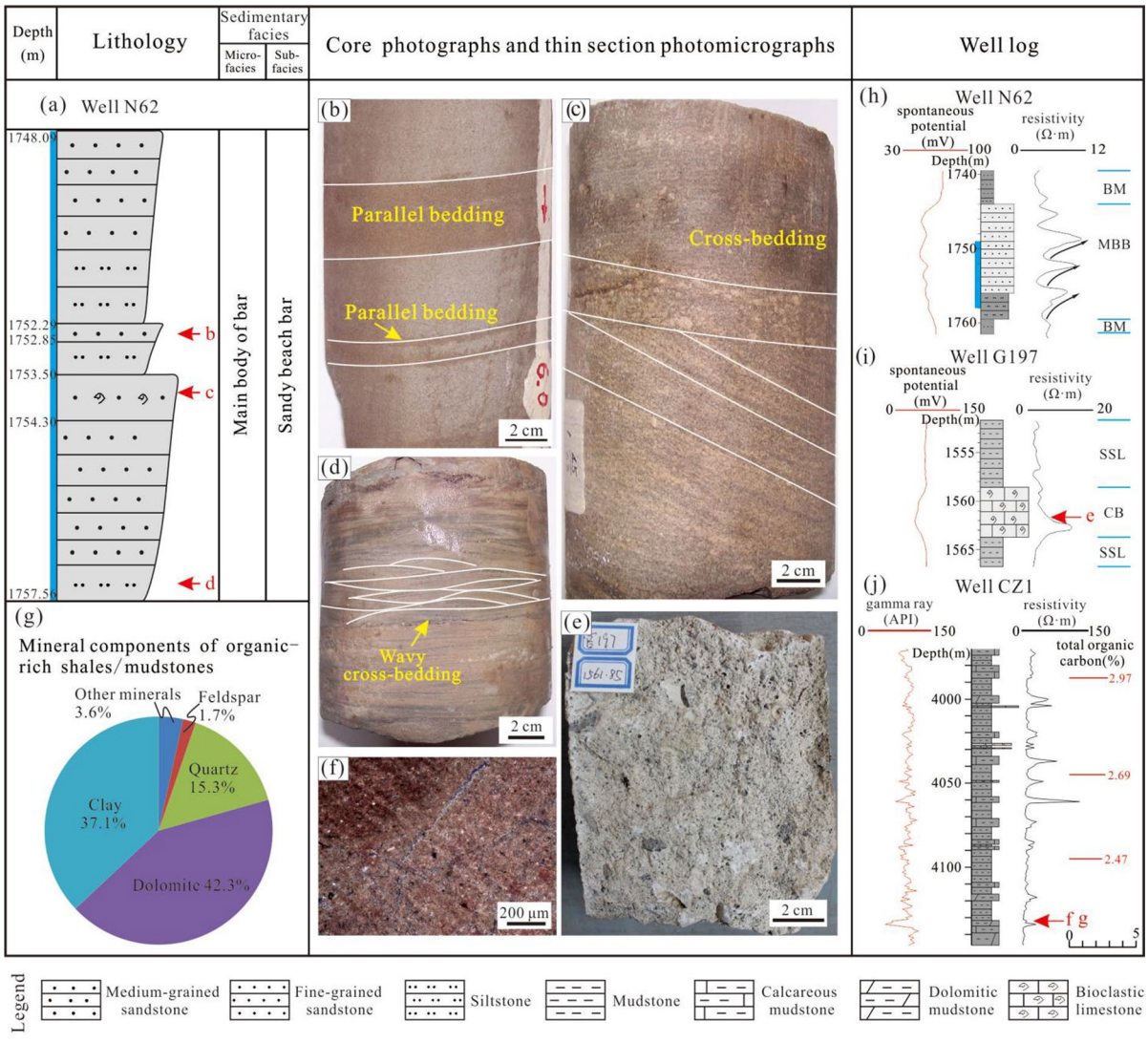

Fig. 8 Cores, thin sections, and well log characteristics of the lake. **a** Stratigraphic column of the sandy beach bar subfacies cores from the Es. **b** Grey fine-grained sandstone with parallel bedding. **c** Grey medium-grained sandstone with cross-bedding (it is hard to determine which type of cross-bedding is based on the features shown in this core), containing abundant gastropod fossils. **d** Grey siltstone with wavy cross-bedding. **e** Grey−white bioclastic limestone. **f** Dolomitic mudstone with fractures. **g** Mineral component content of the dolomitic mudstone. **h** Well log characteristics of sandy beach bar deposits. **i** Well log characteristics of carbonate bank deposits. **j** Well log characteristics and TOC contents of semi-deep to deep lake deposits. The locations of drilling wells are shown in Fig. 1c

magnetite prevail in the Xuxi provenance, with minor rutile and hornblende. Garnet, zircon and haematite dominate in the Dongguang provenance, followed by magnetite and tourmaline (Fig. 9a). The Kongdian provenance can be identified by rock fragment characteristics because it is marked by mainly sedimentary rock fragments. However, the Cangxian provenance is dominated by magmatic rock fragments (Fig. 9a). The sandstone percentage content graph shows that (Fig. 9b) nine provenances are detected

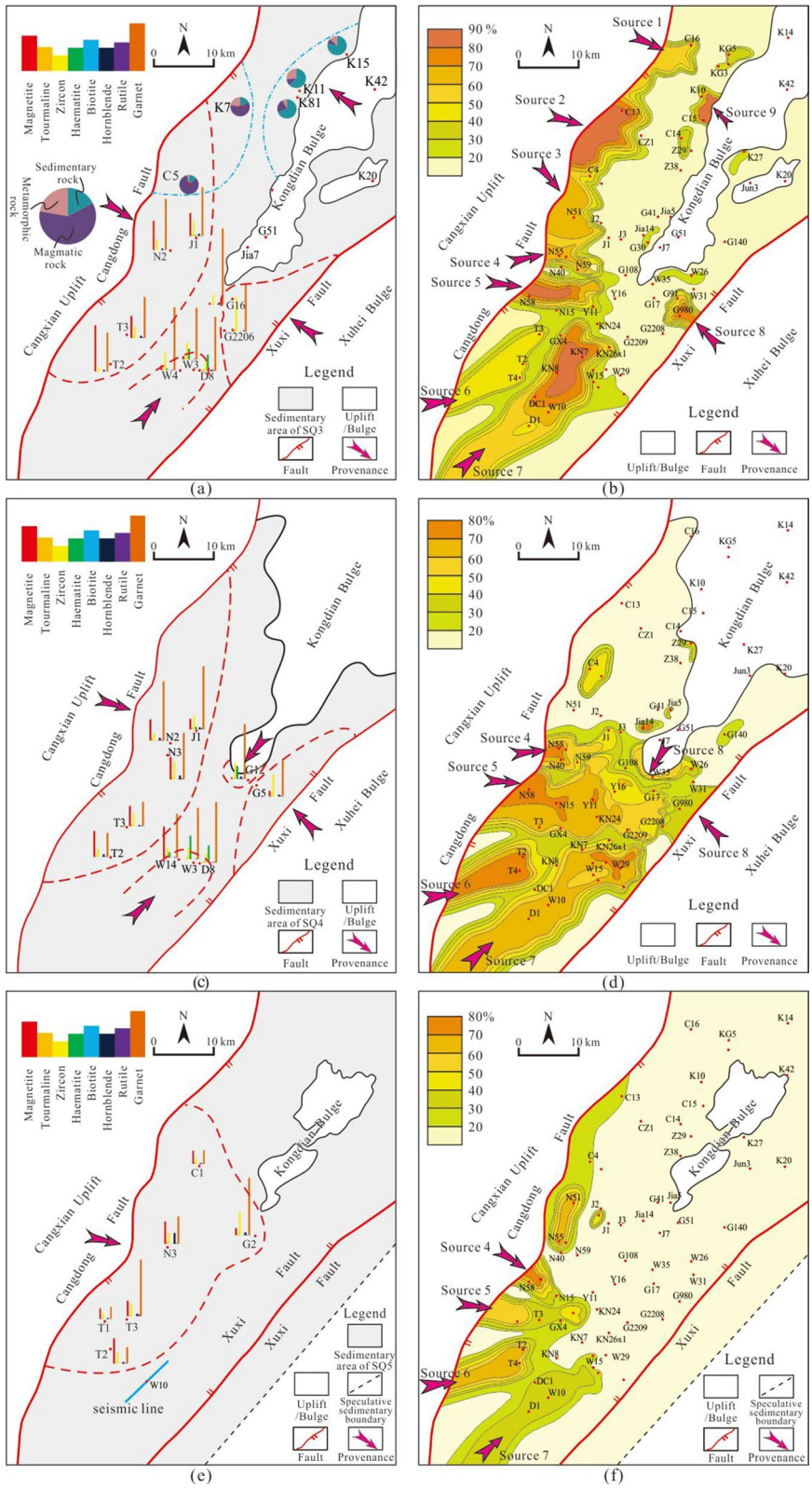

Fig. 9 Heavy mineral characteristics of the CDD (**a** SQ3; **c** SQ4; and **e** SQ5) and contour lines of sandstone percentages (**b** SQ3; **d** SQ4; and **f** SQ5) in the Es of the CDD. **a** contains rock fragments analyses. See Fig. 7m for the seismic profile corresponding to the seismic line in **e**

in the CDD during the depositional period of SQ1. There are two types of sand body dispersion systems. One type is characterized by the development of lateral water systems vertically or obliquely arranged in parallel with the Cangdong fault or the Xuxi fault. The other type is the longitudinal water system, which originates from the high bulge in the south and extends to the low-lying area along the main structural line of the basin. In addition, a short-axis lateral water system occurs in the Kongdian bulge, serving as a local provenance.

Four major provenances are also detected in the CDD during the SQ4 period. The heavy mineral characteristics of the Cangxian provenance, Xuxi provenance and Dongguang provenance are consistent with those of each provenance during the depositional period of SQ3 (Fig. 9c). Garnet, zircon and magnetite dominate in the Kongdian provenance, with minor haematite (Fig. 9c). The contour map of sandstone percentages shows that (Fig. 9d) six provenance mouths formed during the SQ4 period. Sand bodies mainly occur in the southern CDD. Two sand body dispersal systems represent this period. Lateral water systems appear in the hanging walls of the boundary faults. Longitudinal water systems appear in the northern Kongdian bulge and the southern Dongguang bulge, extending along the basin's main structural line.

Based on heavy mineral characteristics, only the Cangxian provenance is identified in the CDD during the SQ5 period, and it has the same heavy mineral characteristics as those in the depositional periods of SQ3 and SQ4 (Fig. 9e). The seismic profile through well W10 shows a significant foreset in the southwest−northeast direction (Figs. 7l, 9e), indicating that the Dongguang bulge in the southwest was also a provenance during this period. The sandstone percentage contour map (Fig. 9f) reveals that the sand bodies decreased in the SQ5 period, and only four provenance mouths were present in the west and in the south. In addition, carbonate rocks are widespread in SQ5, and a large area of bioclastic limestone was deposited at the bottom of SQ5 around the underwater highlands of the Kongdian bulge; the maximum thickness of this limestone is approximately 20 m (Fig. 10), above which dark shale was deposited.

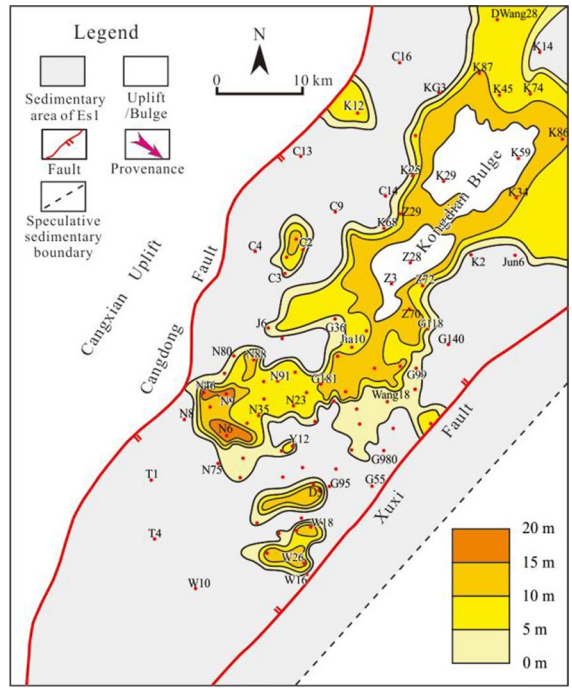

Fig. 10 Contour of SQ5 (Es1) bioclastic limestone thickness

4.4 Distribution of the sedimentary system

The sedimentary system spatial distributions of SQ1–SQ3 are highly similar. Therefore, only SQ3 is analysed to represent the distribution of the entire Es3 sedimentary system.

During the SQ3 period, three fan deltas formed in the northwestern CDD, and one fan delta formed in the eastern margin, with sandstone lobes extending a short distance into the interior sag. Three braided deltas appeared in the southwestern margin, with the delta front extending a long distance into the interior sag. An axial meandering river delta formed on the southern side. Multiple delta fronts were intertwined. Small braided delta and sandy beach bars developed around the Kongdian bulge, along which sandy beach bars present banded distribution characteristics (Fig. 11a).

During the SQ4 period, the lake rapidly shrank, and the water body became shallower. The delta sedimentary system was widespread in the south, while the lacustrine sedimentary system was prevalent

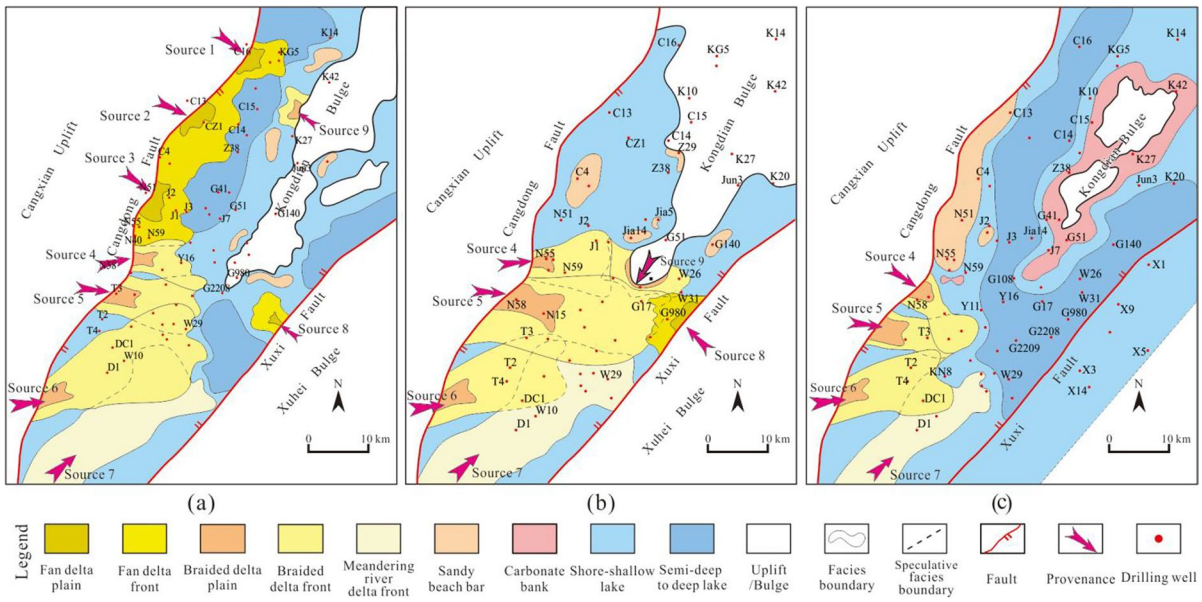

Fig. 11 Sedimentary system distributions of the Es in the CDD. **a** Sedimentary system distribution of SQ3. **b** Sedimentary system distribution of SQ4. **c** Sedimentary system distribution of SQ5

in the north, with the shore-shallow lake and sandy beach bar subfacies dominating. In the southern CDD, braided deltas appeared in the west, fan deltas appeared in the east, and meandering river deltas appeared at the southern end, representing more obvious progradation than during the depositional period of SQ3 (Fig. 11b). Meanwhile, the Kongdian bulge also served as a provenance since it became larger in this period. The braided delta therefore developed from the Kongdian bulge to the southern CDD (Fig. 11b).

During the SQ5 period, the lacustrine basin expanded, and lake facies were widespread. In the southern CDD, a braided delta appeared in the western margin, and a meandering river delta formed in the southern margin. These deltas showed obvious retrogradation compared with the SQ4 period. During this period, the Xuhei bulge did not provide provenance to the sag since it was flooded by the lake. The Kongdian bulge shrank significantly and was surrounded by carbonate banks. Although bioclastic limestone is widespread, it is thin and overlain by thick grey and dark mudstone (Fig. 10). Thus, in the SQ5 sedimentary system distribution map, the carbonate banks appeared only around the Kongdian bulge. In addition, a sandy beach bar appeared in the northwestern CDD (Fig. 11c).

5 Discussion

5.1 Controlling factors of sedimentary characteristics

5.1.1 Tectonic movement

Sequences deposited in the same tectonic stage have similar distribution characteristics of sedimentary systems (Haupert et al. 2016; Li et al. 2019). The distribution characteristics of the sedimentary systems were mostly similar during the SQ1–SQ3 period; therefore, the control of tectonic movement on sedimentary evolution is discussed for three periods, namely, Es3 (SQ1–SQ3), Es2 (SQ4), and Es1 (SQ5).

The burial time−depth map of the Es3 bottom boundary shows that the geomorphologic height significantly differed in the Es3 (SQ1–SQ3) period. Subsidence was the most intense at the bases of downthrown fault walls, and the Cangdong fault and Xuxi fault jointly controlled the geomorphologic characteristics (Fig. 12a). During the Es3 (SQ1–SQ3) period, the activity on the Cangdong

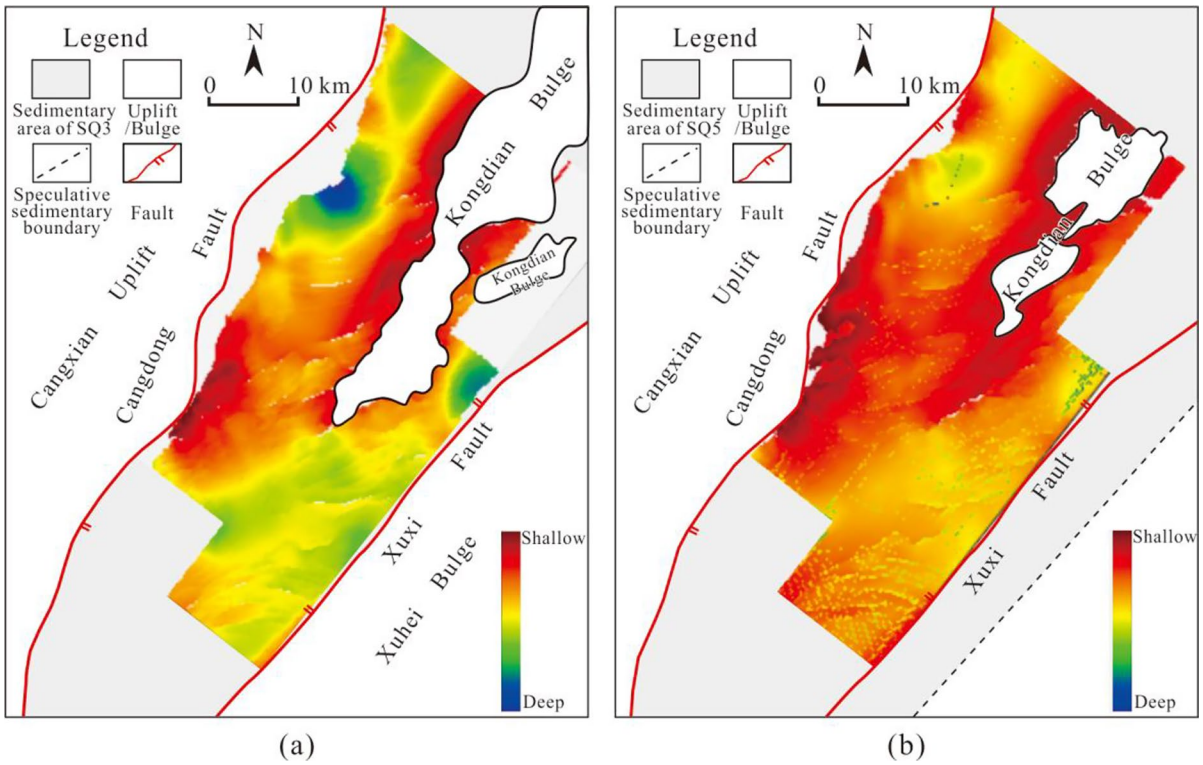

Fig. 12 **a** Burial time−depth plot of the Es3 bottom boundary. **b** Burial time−depth plot of the Es1 bottom boundary

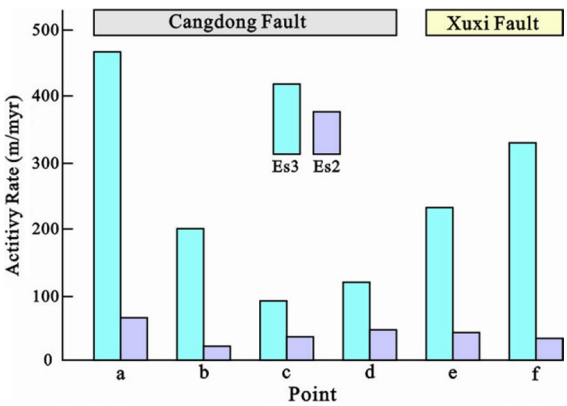

Fig. 13 Boundary fault activity rates in the CDD. Measurement point locations are shown in Fig. 1c

and Xuxi faults was intense, although it varied spatially. The activity rate was generally greater than 200 m/myr on the northern segments of the Cangdong fault and the Xuxi fault, even up to 500 m/myr, although it was generally less than 100 m/myr on the southern segment of the Cangdong fault (Fig. 13). Differential activity rates determined the spatial distribution of the sedimentary systems. There were steep slopes in the hanging walls of the Xuxi fault and the northern Cangdong fault because of the intense activity rates (Figs. 2a, b, 12a); therefore, the geomorphologic heights were quite different between the hanging wall and footwall. Detrital materials directly entered deep water bodies along valleys, and river energy rapidly weakened; therefore, poorly sorted detrital materials accumulated directly near the downthrown walls of the faults. As a result, fan deltas appeared on the hanging walls of the Xuxi fault and the northern Cangdong fault, and these fan deltas extended short distances into the interior sag. The activity was weak on the southern segment of the Cangdong fault; therefore, a gentle slope belt was generated (Fig. 2c, d). Energy attenuation was slower after the river entered the shallow water on a gentle slope, and detrital materials were carried into the interior sag, thereby forming large braided deltas on the western margin of the southern

CDD, which extended farther into the interior sag. The Kongdian bulge, formed by the interaction between the downthrown walls of the two boundary faults, provided local provenance, around which a gentle slope zone appeared. Thus, sandy beach bars and small braided deltas occurred in this flat zone. In addition, the meandering river delta appeared on the inherited gentle slope on the southern margin. Therefore, the control of the abovementioned tectonic movements on the spatial distributions of sedimentary systems was, in essence, controlled by palaeogeomorphologic slopes that formed due to differential faulting activity or fault interactions on the distributions of sedimentary systems, as well as the control of inherited palaeogeomorphologic characteristics on the distributions of sedimentary systems.

During the SQ4 period, boundary faulting activity obviously weakened and showed limited spatial differences, and the maximum activity rate of boundary faults was approximately 80 m/Myr (Fig. 13). The accommodation space in the CDD therefore decreased rapidly, and the Kongdian bulge became larger. The lower growth rate of accommodation space led to the progradation of sand bodies (Gawthorpe et al. 1997; Alves et al. 2003; Catuneanu 2002, 2006; Ji et al. 2013). Therefore, compared to the depositional period of SQ3, deltas in the southern CDD showed obvious progradation during the depositional period of SQ4. However, only a small strip of sandy beach bar developed in the northern CDD, which may have resulted from the decrease in sediment supply to the northern CDD. The sediment supply is discussed in detail in the next section.

During the depositional period of SQ5, boundary faulting activity weakened, and broad crustal thermal subsidence was dominant (Zhang 2018). The control of faults on palaeogeomorphology weakened, and the topography became relatively gentle (Fig. 12b). The superimposed map of the SQ5 bioclastic limestone thickness contour and the SQ5 bottom boundary burial time−depth shows (Fig. 14) that bioclastic limestone generally appeared on the surrounding area of the Kongdian bulge, the nose-shaped bulge of the downthrown wall of the Cangdong fault, and the underwater low bulge of the Cangdong and Nanpi subsags. Compared to the slope in the SQ1–SQ3 period, the slope became

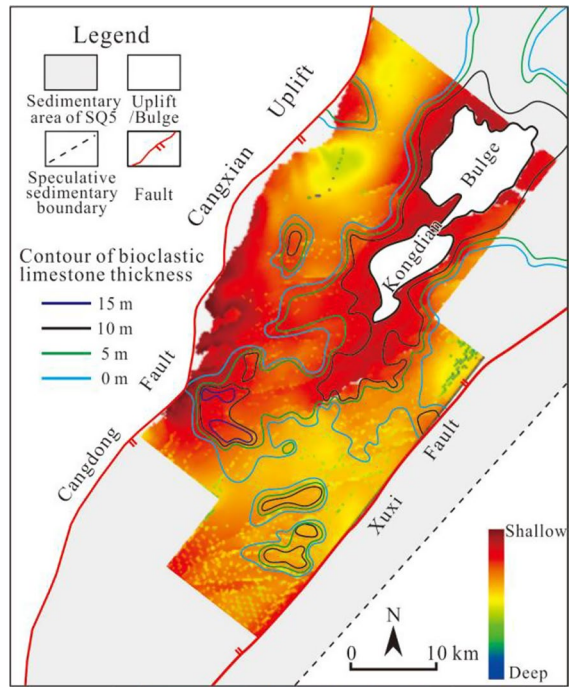

Fig. 14 Superimposed map of the SQ5 (Es1) bioclastic limestone thickness contours and SQ5 (Es1) bottom boundary burial time−depth curve in the CDD

gentler (Fig. 12a, b). When the slope was steep, wave action directly affected the lake shore, and sufficient clastic materials were then generated, which was not conducive to the development of a clean water environment, thereby hindering the formation of carbonate rocks (Liu 2018). The relatively flat topography caused by the weakening of fault activity and the broad crustal thermal subsidence promoted the formation of clean and shallow sedimentary environments at underwater low bulges and provided favourable conditions for the growth of calcareous organisms, thereby enhancing the deposition of bioclastic limestone.

5.1.2 Sediment supply

As mentioned above, during the SQ4 period, progradation took place in the delta in the southern CDD, although the lake dominated in the north, and only a small sandy beach bar appeared. This contrast indicates that there are other factors controlling the sedimentary evolution in addition to the variation in accommodation space caused by changes in

faulting intensity. The evolution of these rocks was also related to the differential supply of sediments (Chen et al. 2020).

The intensity of tectonic movement will influence denudation in the provenance area and thus control the sediment supply intensity and the sedimentary system. The cessation of tectonic movement would have resulted in a gradual erosional decrease in the nearby source area as well as a decrease in the provenance mouths and sediment supply (Pinet and Sourriau 1988; Hou et al. 2019). Compared to the SQ3 period, the depositional periods of SQ4 and SQ5 showed weakened activity along boundary faults; in particular, the activity on the northern Cangdong fault was sharply reduced (Fig. 13). Therefore, the disappearance of the rivers in the three provenance mouths in the northern CDD might have resulted from the decrease or cessation of tectonic movement and further led to changes in sediment supply. The reduction in provenance mouths in the SQ5 period also promoted the formation of warm, clean and shallow sedimentary environments at underwater low bulges and provided favourable conditions for the deposition of bioclastic limestone.

5.1.3 Hydrologic conditions

The salinity of the palaeolake was determined by the V concentration and Sr/Ba value. V concentrations of < 86 ppm, 86–110 ppm and > 110 ppm indicate sea or saline water environments, transitional environments and freshwater environments, respectively (Chen et al. 1997). Sr/Ba values < 0.5, 0.5–1 and > 1 indicate freshwater environments, transitional environments and sea or saline water environments, respectively (Deng and Qian 1993; Ma et al. 2022). The V concentrations of Es3 (SQ1–SQ3) mudstones vary over 51.98–97.71 ppm (average, 65.85 ppm) (Table 1), in which only one sample indicates a transitional environment, while all the others indicate sea or saline water environments. The Sr/Ba values of Es3 (SQ1–SQ3) mudstones vary over 1.07–2.86

Table 1 Concentrations of minor elements (ppm) and the related analytical results in the Es

Strata	Well	Depth (m)	Lithology	Minor elements (ppm)			Sr/Ba
				V	Sr	Ba	
Es3 (SQ1–SQ3)	C9	3128.82	Dark mudstone	68.26	1159.57	682.23	1.70
	C9	3129.37		59.16	1416.32	730.89	1.94
	C9	3129.81		69.57	1162.96	683.26	1.70
	C9	3140.36		58.98	1406.87	533.42	2.64
	C9	3140.59		63.41	1194.92	575.94	2.07
	C9	3140.79		66.28	970.83	482.79	2.01
	C9	3141.83		66.26	1216.49	564.82	2.15
	C9	3142.70		59.96	1520.08	531.26	2.86
	C9	3144.43		64.37	1026.04	390.45	2.63
	C9	3145.33		63.06	1096.22	516.61	2.12
	W33	2955.31		64.49	872.18	406.07	2.15
	W33	2957.81		75.02	762.01	416.87	1.83
	W19	2991.59		61.90	468.23	380.56	1.23
	W19	2996.51		97.71	343.30	318.51	1.08
	X4	2993.25		75.89	344.87	321.06	1.07
	X4	2995.88		58.39	533.42	356.72	1.50
	X4	2997.53		51.98	750.51	444.93	1.69
	X4	2998.11		60.63	536.83	365.74	1.47
Average				65.85	932.31	483.45	1.88
Es1 (SQ5)	G197	1547.88	Argillaceous limestone	45.99	1977.76	295.91	6.68
	G197	1559.66	Bioclastic limestone	15.50	1529.19	531.20	2.88
	G197	1563.35	Bioclastic limestone	7.70	1320.27	839.34	1.57
Average				23.06	1609.07	555.48	3.71

(average, 1.88), indicating a sea or saline water environment (Table 1). The V concentrations of Es1 (SQ5) limestones vary over 7.7–45.99 ppm (average, 23.06 ppm), and the Sr/Ba values of Es1 (SQ5) limestones vary over 1.57–6.68 (average, 3.70) (Table 1). All samples indicate sea or saline water environments. In conclusion, the CDD was a high-salinity lake during the Es3 (SQ1–SQ3) and Es1 (SQ5) periods.

High-salinity lakes may be related to hot and arid climates, in which lake water continuously evaporates, leading to higher salinity. However, palynological assemblages indicate that the CDD had a humid climate during the Es3 (SQ1–SQ3) and Es1 (SQ5) periods (Tong and Gu 1985), which was obviously not conducive to the formation of high-salinity lakes. High-salinity lakes can also be caused by the injection of additional salts into the lake; for example, offshore lakes are occasionally affected by sea water intrusion. Based on palaeontological, mineral, and geochemical characteristics, extensive sea water intrusions are considered to have occurred in the BBB during the depositional periods of Es3 and Es1 (Chen 1985; Gao 2003; Chen et al. 2012; Wei et al. 2018). Similarly, the chlorite, collophane, coccoliths, trace element concentrations, strontium isotope values (Chen et al. 2012) and palaeontological characteristics (Chen 1985) of the CDD also indicate that significant sea water intrusions occurred during the depositional periods of Es3 (SQ1–SQ3) and Es1 (SQ5). Therefore, the salinization of the lake in the CDD may be caused by sea water intrusion. The BBB was a coastal lake during the Eocene (Fig. 15a). Wei et al. (2018) proposed two mechanisms as to the causes of sea water intrusion in the lake environment of the BBB. (1) Tectonic mechanism, it is considered that the tectonic subsidence of structures at the junction of the BBB and Pacific Ocean resulted in sea water intrusion (Fig. 15b); (2) Eustatic mechanism, it is believed that global sea level rise caused sea water intrusion (Fig. 15c). There are many subuplifts and subbasins in the BBB (Fig. 1a). The Huanghua subbasin, including the CDD, is in the middle of the BBB and opens up in a trumpet shape from southwest to northeast (Fig. 1a, b). Based on the distribution of subuplifts and subbasins (Fig. 1a), the sea water may intruded from the northeast direction of the CDD (Fig. 16a, c).

The impact of high-salinity lake water on the sedimentary system of the Es is mainly revealed by the following features. First, calcium carbonate was easily oversaturated and precipitated in a high-salinity water environment. In the low-relief uplifted area, where calcareous organisms were productive, the combination of biological and chemical effects promoted the deposition of bioclastic limestone. Second, high-salinity water promoted the accumulation of dolomite and calcite in dark mudstone (Fig. 8f, g). Third, because the high-salinity water was rich in calcium ions, arene oolites frequently appeared in the sandstone of the mouth bars and sandy beach bars after reforming in lake currents (Figs. 6m, 7f, h).

Lambiase (1990) and Hou et al. (2019) considered that lacustrine and related sedimentary systems would change to fluvial-floodplain sedimentary systems during the late rifting period. However, the CDD showed a reverse change. During the SQ5 period, when rifting weakened, the accommodation space increased significantly, and the lacustrine sedimentary system dominated (Fig. 11c). At this time, the palaeogeomorphology of the BBB was gentle; the entire BBB was dominated by lacustrine sediments, and bioclastic limestone and dark mudstone/shale were widespread, which can be contrasted throughout the entire BBB (Zhu et al. 2008; Liu et al. 2020b). This situation might have been associated with the extensive intrusion of seawater caused by regional thermal subsidence or global sea level rise. The accommodation space of the basin therefore increased in the SQ5 period, which in turn led to obvious retrogradation of the delta.

5.2 Depositional model

The CDD experienced intense rifting in the SQ1–SQ3 period, weakened rifting in the SQ4 period, and weakened rifting and dominant broad crustal thermal subsidence in the SQ5 period. During the SQ1–SQ4 period, clastic rock sedimentary systems dominated the CDD. The palaeogeomorphology formed by differential faulting activity or fault interactions and inherited palaeogeomorphology jointly controlled the types and distributions of sedimentary systems (Wu et al. 2015a, b; Li et al. 2019, 2022). The changes in accommodation space and sediment supply caused by the changes in the boundary fault activity resulted in deltas that show progradation or disappear in SQ4 (Fig. 16a, b). Affected by the high concentrations of

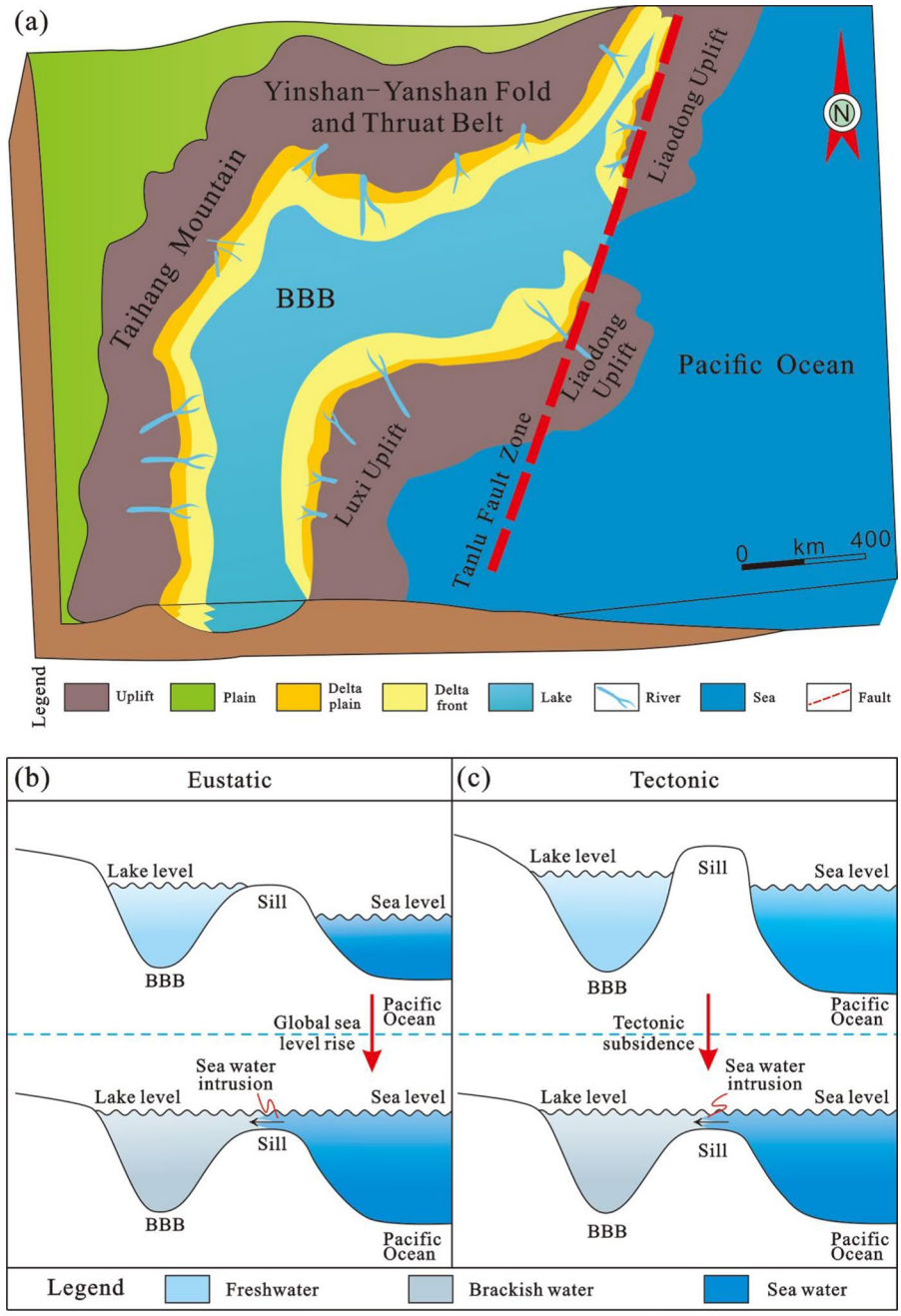

Fig. 15 **a** Palaeogeography of the BBB during the Eocene. **b** Model of the eustatic mechanism for sea water intrusion. **c** Model of the tectonic mechanism for sea water intrusion. **a–c** are modified after Wei et al. (2018)

calcium and magnesium ions in high-salinity lake water during the depositional periods of SQ1–SQ3 and SQ5, lacustrine argillaceous sediments were rich in carbonate minerals, and sandstone was rich in arene oolites. During the depositional period of SQ1–SQ3, due to sufficient terrigenous material input and large palaeogeomorphologic relief, a clean lake environment could not have formed in underwater highlands. Therefore, sandy beach bars rather than carbonate banks developed around the Kongdian bulge (Fig. 16a). During the depositional period of SQ5, the topography became gentle, the sediment supply weakened, and the large-scale sea water intrusion increased the accommodation space. As a result, obvious retrogradation occurred in the delta. Warm, clean and shallow sedimentary

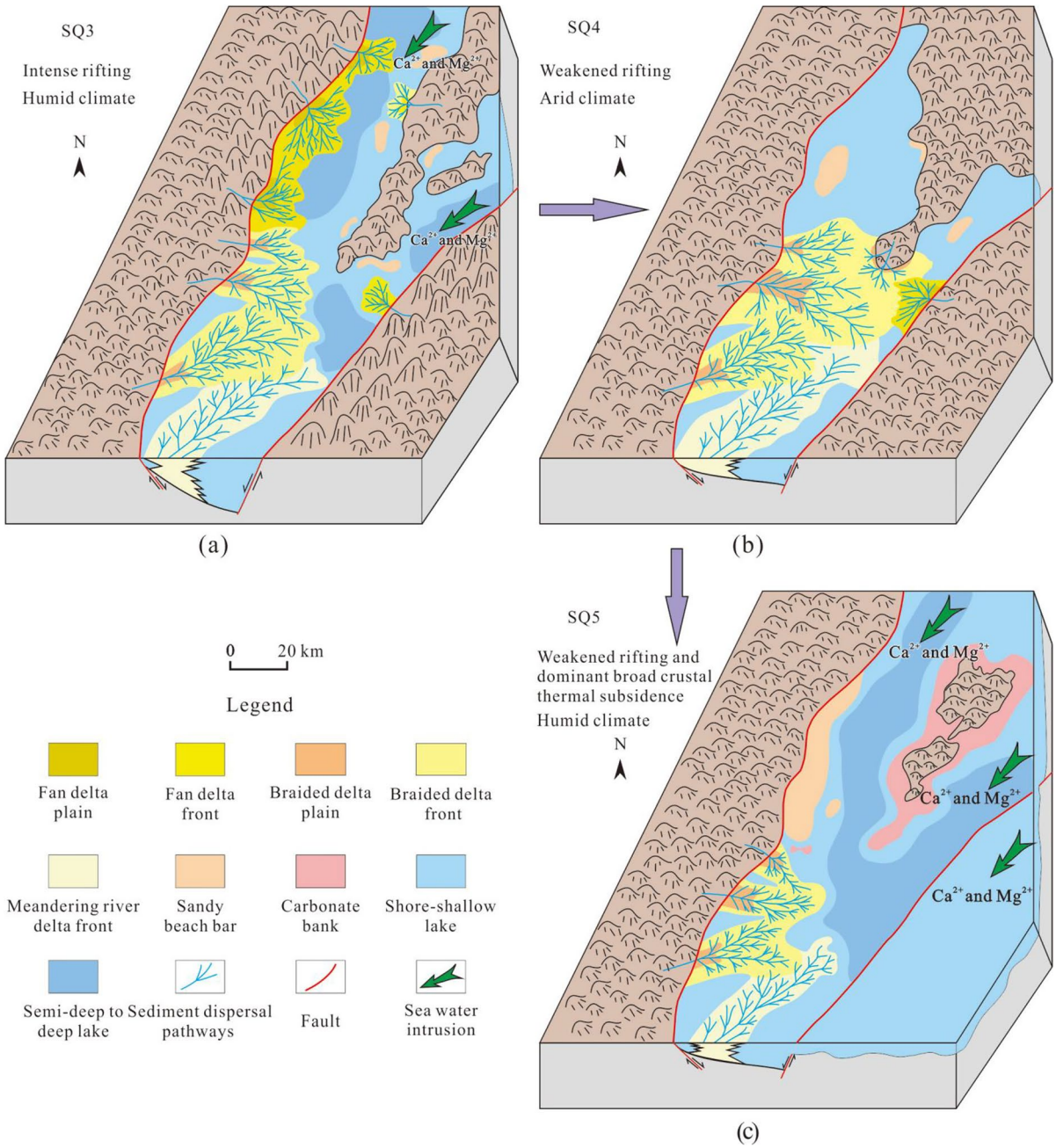

Fig. 16 Depositional model of the Es in the CDD. **a** Depositional model of SQ3. **b** Depositional model of SQ4; **c** depositional model of SQ5

environments formed on underwater low bulges far from the provenance mouths, which promoted the growth of calcareous organisms. The calcareous biological shells and their debris formed the framework of bioclastic limestone. At the same time, calcium carbonate precipitated after it was saturated in the high-salinity lake. Therefore, under the joint action of biological and chemical factors, bioclastic limestone formed (Fig. 16c).

According to the research results, the clastic rock sedimentary systems in the continental rift basin mainly appear in the rifting period with intense fault activity, which is mainly affected by tectonic movement and sediment supply; bioclastic limestones mainly develop on gentle low bulges and during periods with less terrigenous material input. In addition, high-salinity lake water is also a vital factor affecting the deposition of carbonate rocks in continental rift basins.

6 Conclusion

Es is divided into five 3rd-order sequences: Es3 corresponds to SQ1, SQ2, and SQ3, from bottom to top; Es2 corresponds to SQ4; and Es1 corresponds to SQ5. Fan deltas, braided deltas, meandering river deltas, and lakes are identified in the Es in the CDD. Clastic rock sedimentary systems developed during the depositional period of SQ1–SQ4, while clastic rock and carbonate rock sedimentary systems developed simultaneously during the depositional period of SQ5.

Tectonic movement, sediment supply, and hydrologic conditions jointly controlled the depositional process of the Es in the CDD. During the SQ1–SQ4 period, the palaeogeomorphology formed by differential faulting activity or fault interactions, as well as the inherited palaeogeomorphology, determined the spatial distributions of the different sedimentary systems, and the changes in accommodation space and sediment supply caused by tectonic movement led the delta to prograde or disappear over time. During the SQ5 period, rifting weakened, broad crustal thermal subsidence was dominant, the sediment supply decreased, and large-scale seawater intrusion increased the accommodation space; thus, obvious retrogradation occurred in the delta. Meanwhile, the high-salinity lake enriched the environment with abundant calcium ions, which promoted the formation of the SQ5 carbonate rock.

Author contributions Conceptualization: SZ, YL; Methodology: YX, XP; Formal analysis and investigation: TZ, LM, XW, PY; Writing—original draft preparation: SZ; Writing—review and editing: YL, XY; Funding acquisition: YL; Resources: XP. All authors read and approved the final manuscript.

Funding This study was funded by the project of the Dagang Oilfield Company, PetroChina (No. DGYT-2018-JS-289), the National Natural Science Foundation of China (No. 42202132) and the Science and technology Plan Project of Sichuan Province (No. 22NSFSC3942).

Data availability All data generated or analysed during this study are included in this article.

Declarations

Ethics approval Not applicable.

Consent for publication Not applicable.

Competing interest All authors declare that there are no conflict of interest.

References

Allen MB, Macdonald DIM, Zhao X et al (1997) Early Cenozoic two-phase extension and late Cenozoic thermal subsidence and inversion of the Bohai Basin, northern China. Mar Pet Geol 14:951–972

Alves TM, Manuppella G, Gawthorpe RL et al (2003) The depositional evolution of diapir- and fault-bounded rift basins: examples from the Lusitanian Basin of West Iberia. Sediment Geol 162(3–4):273–303

Bayet-Goll A, Geyer G, Daraei M (2018) Tectonic and eustatic controls on the spatial distribution and stratigraphic architecture of late early Cambrian successions at the northern Gondwana margin: the siliciclastic-carbonate successions of the Lalun Formation in central Iran. Mar Pet Geol 98:199–228

Blair TC (1987) Tectonic and hydrologic controls on cyclic alluvial fan, fluvial, and lacustrine rift-basin sedimentation, Jurassic-Lowermost Cretaceous Todos Santos Formation, Chiapas, Mexico. J Sediment Res 57(5):845–862

Catuneanu O (2002) Sequence stratigraphy of clastic systems: concepts, merits, and pitfalls. J Afr Earth Sci 35(1):1–43

Catuneanu O (2006) Principles of sequence stratigraphy. Elsevier, Amsterdam

Catuneanu O, Abreu V, Bhattacharya JP et al (2009) Toward the standardization of sequence stratigraphy. Earth Sci Rev 92(1–2):1–33

Catuneanu O, Galloway WE, Kendall CGSC et al (2011) Sequence stratigraphy: methodology and nomenclature. Newsl Stratigr 44(3):173–245

Chen C, Huang J, Chen J et al (1984) Depositional models of Tertiary rift basins, eastern China, and their application to petroleum prediction. Sediment Geol 40(1–3):73–88

Chen ZQ (1985) On sedimentary conditions of 3rd member Shahejie Formation (Palaeogene) in Huanghua Depression, Hebei Province. Mar Geol Q Geol 5(2):37–50 (**in Chinese with English abstract**)

Chen ZY, Chen ZL, Zhang WG (1997) Quaternary stratigraphy and trace element indicates of the Yangtze delta, eastern China, with special reference to marine transgressions. Quat Res 47(2):181–191

Chen SY, Li C, Yang YQ et al (2012) Depositional environment of the lacustrine dolomite in Sha-1 lower submember of the Qikou Sag, Huanghua Depression. Acta Geol Sin 86(10):1679–1687 (**in Chinese with English abstract**)

Chen L, Ji HC, Zhang L et al (2020) Rift activity and sequence stratigraphy of the Oligocene Dongying Formation in the Nanpu Sag, eastern China: Implications for rift sequence stratigraphy in lacustrine basins. Geol J 55(2):1163–1178

Collinson JD, Mountney NP, Thompson DB (2006) Sedimentary structures (3rd editon). Terra Publishing, Harpenden

Deng HW, Qian K (1993) Sedimentary geochemistry and environmental analysis. Gansu Science and Technology Press, Lanzhou (**in Chinese with English abstract**)

Gao XX (2003) Oil and natural gas geology in Huanghua depression. Petroleum Industry Press, Beijing (**in Chinese with English abstract**)

Gawthorpe RL, Leeder MR (2000) Tectono-sedimentary evolution of active extensional basins. Basin Res 12(3–4):195–218

Gawthorpe RL, Sharp I, Underhill JR et al (1997) Linked sequence stratigraphic and structural evolution of propagating normal faults. Geology 25(9):795–798

Ge JW, Zhu XM, Wang R et al (2018) Tectono-sedimentary evolution and hydrocarbon reservoirs in the Early Cretaceous Tanan Depression, Tamtsag Basin, Mongolia. Mar Pet Geol 94:43–64

Gierlowski-Kordesch EH (2010) Lacustrine carbonates. In: Alonso-Zarza AM, Tanner LH (eds) Carbonates in continental settings: facies, environments, and processes. Elsevier, Amsterdam, pp 1–101

Goswami S, Ghosh P (2020) Evolution of sedimentation pattern in a continental rift basin of India, between the Late Triassic and the early Middle Jurassic: tectonic and climatic controls. Sediment Geol 405:105679

Hanneman DL, Wideman CJ (2010) Chapter 5 continental sequence stratigraphy and continental carbonates. In: Alonso-Zarza AM, Tanner LH (eds) Carbonates in continental settings: geochemistry, diagenesis and applications. Elsevier, Amsterdam, pp 215–273

Haughton PDW, Todd SP, Morton AC (1991) Sedimentary provenance studies. Geol Soc Lond Spec Publ 57:1–11

Haupert I, Manatschal G, Decarlis A et al (2016) Upper-plate magma-poor rifted margins: stratigraphic architecture and structural evolution. Mar Pet Geol 69:241–261

Holmes A (1965) Principles of physical geology. Thomas Nelson and Sons, London

Hou YC, Wang HY, Fan TL et al (2019) Late syn-rift sequence architecture and sedimentary evolution of a continental rift basin: a case study from Fulongquan Depression of the Songliao Basin, northeast China. Mar Pet Geol 100:341–357

Ji HC, Jia HB, Sun SM et al (2013) Tectonics-palaeogeomorphology in rift basins: controlling effect on the sequence architecture. Pet Sci 10(4):458–465

Jia YC, Lin CS, Erikssonc KA et al (2019) Fault control on depositional systems and sequence stratigraphic architecture in a multiphase, rifted, lacustrine basin: a case study from the paleogene of the central Bohai Bay Basin, northeast China. Mar Pet Geol 101:459–475

Lambiase JJ (1990) A model for tectonic control of lacustrine strategraphic sequences in continental rift basin. In: Katz BJ (ed) Lacustrine basin exploration: case studies and modern analogs. American Association of Petroleum Geologists, Tulsa, pp 265–276

Leeder MR, Gawthorpe RL (1987) Sedimentary models for extensional tilt-block/half graben basins. Geol Soc Lond Spec Publ 28(1):139–152

Li XP, Wang H, Gan HJ et al (2019) Stratigraphic charactertistic and tectonic control on the paleogene sedimentary evolution of the Baxian Half-graben, Bohai Bay Basin, east China. J Pet Sci Eng 181:106145

Li Q, Zhang ZL, Zhang J (2022) Characteristics of sedimentary differential response for multi-episode rifting cycles in lacustrine rift basin: a case study of the Palaeogene Baxian sag in the Bohai Bay Basin. Mar Pet Geol 136:105426

Liu SQ (2018) Sedimentary characteristics of lacustrine carbonates in the upper fourth member of shahejie formation (Es4s), western Dongying depression. Dissertation, China University of Geosciences. (**in Chinese with English abstract**)

Liu ZC, Liu GQ, Ge W et al (2010) Hydrocarbon accumulation conditions and exploration region of Es sags in Kongnan Area. Nat Gas Geosci 21(4):606–611 (**in Chinese with English abstract**)

Liu SQ, Jiang ZX, He YB et al (2020a) Geomorphology, lithofacies and sedimentary environment of lacustrine carbonates in the Eocene Dongying Depression, Bohai Bay Basin, China. Mar Pet Geol 113:104125

Liu L, Chen HD, Wen HG et al (2020b) Facies architecture and sediment infilling processes in intrabasinal slope belts of lacustrine rift basins, Zhanhua Depression, Bohai Bay Basin. Mar Pet Geol 112:104089

Ma Q, Zhou YQ, Mu HY (2022) Geochemisty of the Laiyang Group from outcrops and Lingke-1 core on Lingshan Island, Shandong Province, Eastern China: implications for provence, tectonic setting and palaeo-environment. Geol Mag 159:37–54

McPherson JG, Shanmugam G, Moiola RJ (1987) Fan-deltas and braid deltas: varieties of coarse-grained deltas. Geol Soc Am Bull 99(3):331–340

McPherson JG, Shanmugam G, Moiola RJ (1988) Fan deltas and braid deltas: conceptual problems. In: Nemec W, Steel RJ (eds) Fan deltas: sedimentology and tectonic settings. Blackie and Son, Glasgow, pp 14–23

Miall AD (1984) Principles of sedimentary basin analysis. Springer, New York

Middleton GV (1973) Johannes Walther's law of correlation of facies. Geol Soc Am Bull 38:979–988

Morley CK (2002) Evolution of large normal faults: evidence from seismic reflection data. AAPG Bull 86(6):961–978

Muniz MC, Bosence DW (2018) Lacustrine carbonate platforms: facies, cycles, and tectonosedimentary models for the presalt Lagoa Feia Group (lower Cretaceous), Campos basin, Brazil. AAPG Bull 102(12):2569–2597

Northrup CJ, Royden LH, Burchfiel BC (1995) Motion of the Pacific plate relative to Eurasia and its potential relation to Cenozoic extension along the eastern margin of Eurasia. Geology 23(8):719–722

Olsen PE (1990) Tectonic, climatic, and biotic modulation of lacustrine ecosystems examples from Newark Supergroup of eastern North America. In: Katz BJ (ed) Lacustrine basin exploration: case studies and modern analogs. American Association of Petroleum Geologists, Tulsa, pp 209–224

Pinet P, Sourriau M (1988) Continental erosion and large-scale relief. Tectonics 7(3):563–582

Ren JY, Tamaki K, Li ST et al (2002) Late mesozoic and cenozoic rifting and its dynamic setting in Eastern China and adjacent areas. Tectonophysics 344(3–4):175–205

Rosendahl BR (1987) Architecture of continental rifts with special reference to east Africa. Annu Rev Earth Planet Sci 15(1):445–503

Song F, Su NN, Yang SC et al (2018) Sedimentary characteristics of thick layer lacustrine beach-bars in the Cenozoic Banqiao Sag of the Bohai Bay Basin, East China. J Asian Earth Sci 151:73–89

Sopeña A, Sánchez-Moya Y (1997) Tectonic systems tract and depositional architecture of the western border of the Triassic Iberian trough (central Spain). Sediment Geol 113(3):245–267

Tong LF, Gu RG (1985) Lower tertiary Biota and Environment of Huanghua Basin. Earth Sci J China Univ Geosci 10(2):1–7 (**in Chinese with English abstract**)

Wang H, Jiang S, Huang CY et al (2011) Differences in sedimentary filling and its controlling factors in rift lacustrine basins, East China: a case study from Qikou and Nanpu sags. Front Earth Sci 5(1):82–96

Wang HY, Fan TL, Wu Y (2015) The subsurface structure and stratigraphic architecture of rift-related units in the Lishu Depression of the Songliao Basin, China. J Asian Earth Sci 99:13–29

Watson MP, Hayward AB, Parkinson DN et al (1987) Plate tectonic evolution, basin development and petroleum source rock deposition onshore China. Mar Pet Geol 4:205–225

Wei W, Algeo TJ, Lu YB et al (2018) Identifying marine incursions into the Paleogene Bohai Bay Basin lake system in northeastern China. Int J Coal Geol 200:1–17

Wu D, Zhu XM, Li Z et al (2015a) Depositional models in Cretaceous rift stage of Fula sag, Muglad Basin, Sudan. Pet Explor Dev 42(3):348–357

Wu D, Zhu XM, Su YD et al (2015b) Tectono-sequence stratigraphic analysis of the Lower Cretaceous Abu Gabra Formation in the Fula Sub-basin, Muglad Basin, southern Sudan. Mar Pet Geol 67:286–306

Xie XN, Ren JY (2013) Principles of sedimentary basin analysis. China University of Geosciences Press, Wuhan (**in Chinese**)

Yang XB, Wang HY, Li ZY (2021) Tectonic-sedimentary evolution of a continental rift basin: a case study of the Early Cretaceous Changling and Lishu fault depressions, southern Songliao Basin, China. Mar Pet Geol 128:105068

Ye L, Zhang JX, Lu GC et al (2013) Paleogene structure-stratigraphic framework and multiple episode evolution in Kongnan Area, Huanghua Depression. Earth Sci J China Univ Geosci 38(2):379–389 (**in Chinese with English abstract**)

Zhang S (2018) Effect on sedimentation of paleogene fault activity in the southern Huanghua Basin. Dissertation, China University of Petroleum. (**in Chinese with English abstract**)

Zhao XZ, Zhou LH, Pu XG et al (2018) Development and exploration practice of the concept of hydrocarbon accumulation in rifted-basin troughs: a case study of Paleogene Kongdian Formation in Cangdong sag, Bohai Bay Basin. Pet Explor Dev 45(6):1166–1176

Zhao XZ, Zhou LH, Pu XG et al (2019) Exploration breakthroughs and geological characteristics of continental shale oil: a case study of the Kongdian Formation in the Cangdong Sag, China. Mar Pet Geol 102:544–556

Zhu XM (2008) Sedimentary petrology, 4th edn. Petroleum Industry Press, Beijing

Zhu XM, Dong YL, Yang JS et al (2008) Sequence stratigraphic framework and distribution of depositional systems for the Paleogene in Liaodong Bay area. Sci China Ser D Earth Sci 51(Supp. II):1–10